Chemistry–A European Journal
Research Article
doi.org/10.1002/chem.202400563
Chemistry Europe
European Chemical Societies Publishing
www.chemeurj.org

N,N'-Diaryl-Sulfurdiimides are Strongly Redox Tuned

Nathan D. D. Hill[a] and René T. Boeré*[a]

The synthesis and extensive characterization of nine aryl sulfur diimides (SDIs, Ar–NSN–Ar) are presented with a robust computational and experimental investigation of the fundamental properties of these important members of the thiazyl family of compounds, with particular attention paid to their highly tunable electrochemical behaviour. This is the first work to undertake a systematic comparison of the electrochemical profiles of a coherent series of SDIs to demonstrate and quantify the response of their reduction potentials to substituent electron-donating and -withdrawing properties. This effect is found to be not only exceptionally strong, but also correlates very closely with computed orbital energies. Electron paramagnetic resonance spectroscopy is used to determine the nature, localization, and qualitative lifetimes of the radical anions of SDIs. This work also addresses significant misconceptions about physical properties of SDIs. Experimental data and modern computational methods are employed to provide a resolute answer to the long-standing contention of the solution-state conformations of SDIs, and to correct historical mistakes in the assignment of infrared spectroscopic data. High-quality crystal structures of all SDIs in this work showcase the utility of the recently introduced structural refinement software NoSpherA2, enabling full anisotropic refinement of H-atoms with accurate C–H bond lengths.

Introduction

Sulfur diimides (SDIs, R–NSN–R) are imines of sulfur dioxide[1] (Figure 1) and were entirely unknown until the first report of the isolation of ^{n}Bu–NSN–^{n}Bu in an historic paper by Becke-Göhring and Weis in 1956,[2] soon followed by similar compounds with $(CH_3)_3Si$–NSN–$Si(CH_3)_3$,[3] ^{t}Bu–NSN–^{t}Bu,[4] and the first aromatic derivative (Ph–NSN–Ph).[5] An ongoing interest in inorganic chemistry is their anionic derivatization in the syntheses of diimidosulfinates, $[(R'N)_2SR]^-$, and triimidosulfinates, $[(R'N)_3S]^-$.[6] The latter have recently been developed as ligands for single-molecule magnets.[6c] *Bis*-trimethylsilyl SDI is important enough to be commercially available and serves as a major synthon for unsaturated sulfur-nitrogen chains and heterocycles.[1,7] The organic chemistry of SDIs has been reviewed repeatedly,[8] and has recently been revived intensively due to significant advances in pharmaceutical applications.[9] A reliable thermodynamic scale has been developed for the replacement of the SO bonds in SO_2 with SNR groups.[10] The nature of the NS bonds in SDIs has been discussed in great depth[11] but is now definitively confirmed to be of the heteroallylic nature shown at the bottom of Figure 1;[11b] in graphical schemes the shorthand partially dashed double line notation has been adopted, but in text, whether written NSN or –NSN–, this heteroallylic character will always be intended.

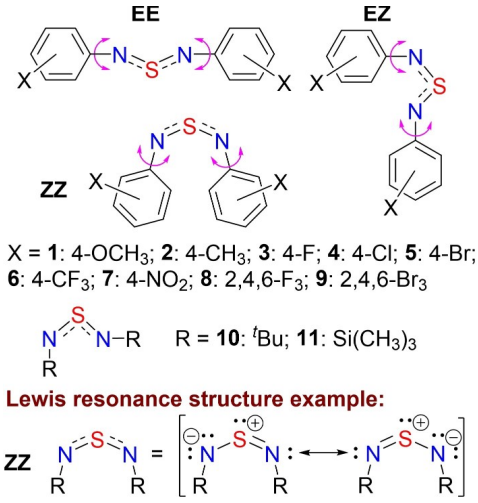

Figure 1. Isomers and conformations in aryl sulfur diimides and compound identification codes. The resonance structures corresponding to the simplified bonding notation is shown for Z/Z as an example (see text). Double-headed arrows around the N–C bonds indicate the C–C–N–S torsions.

Sulfur diimides are capable of incorporating an extensive range of substituents. A great number and variety of SDIs have been (separately or in collaboration) synthesized by Herberhold, Hörhold, and Wrackmeyer, including organic alkyl, perfluoroalkyl, aryl or perfluoroaryl R-groups, and heteroatom groups such as silyl, phosphinyl, germanyl, etc.[3b,12] A wide variety of mostly aryl SDIs was developed by the Russian school led by Zibarev.[13] A key driving force for much of this work was the exploration of -{NSN-}$_\infty$ chains to mimic or model the behaviour of $(SN)_x$.[14] Recently, –(Ar–NSN–Ar–)$_\infty$chain polymers have been reported, after a long unsuccessful search for such species.[15] Closely

[a] N. D. D. Hill, Prof. Dr. R. T. Boeré
Department of Chemistry and Biochemistry and The Canadian Centre for Research in Advanced Fluorine Technologies, University of Lethbridge, 4401 University Dr. W, Lethbridge, AB, Canada T1K3M4
E-mail: boere@uleth.ca

Supporting information for this article is available on the WWW under https://doi.org/10.1002/chem.202400563

related to these achievements is the report of an unusual SDI that appears to be dominated by C_{aryl}=N bonds and consequently possesses very long N–S bonds.[16] Cyclic diimides are known for all chalcogens,[1] and fused-ring aryl-1,2,5-chalcogenadiazoles, **12** (Figure 2), are undoubtedly the largest of this very important and heavily studied class of SDIs. However, the electronic structures and resultant properties (especially luminescence) of such cyclic systems is dominantly a function of their modified aryl rings rather than the chalcogen atom and as such will not be further discussed in this article;[17] for the role of the chalcogen in **12** see ref. [18].[18]

As shown in Figure 1, three conformations must be considered for SDIs, E/E, E/Z, and Z/Z, making them much more complex than SO_2, although the bonding in the two systems is now recognized to be analogous.[19] Whereas the majority of coordination complexes of SDIs, with the exception of late transition metals, are chelated structures that mandate the E/E conformation, E/Z and Z/Z are common for the free molecules. Some early results already hinted that chelated SDIs can sometimes function as redox non-innocent ligands in coordination complexes. Hunter et al. (1980) and Klein et al. (1996) showed by electron paramagnetic resonance (EPR) spectroscopy that several chemically or electrochemically reduced complexes localize the electron density of the added electron primarily on the SDI ligand, thereby leaving the oxidation state of the metal formally unchanged.[20] Redox-active ligands have had a profound impact on coordination chemistry, and made possible reactivities that were previously inaccessible, or prohibitively expensive. They have many uses, including, though certainly not limited to: efficient electrode materials for lithium ion batteries,[21] strong dyes and pigments,[22] and semiconducting nanosheets.[23] Perhaps most notable is the transformative potential of complexes with redox-active ligands in the field of catalysis. Brookhart et al. tested the activity of an iron-based catalyst with a redox-active ligand system for synthesizing α-olefins, and found the activity to be comparable to that of precious metal catalysts, with excellent selectivity.[24]

Recently, we demonstrated approximately one electron reduction of coordinated **11** at several lanthanocene derivatives [$LnCp^*_2(Me_3SiNSNSiMe_3)$],[25] **13** (Figure 2), which are the first structurally characterized complexes of SDI radical anions,[1,26] supported by a preliminary voltammetric study of **11**. Similarly, Kaleta et al.[27] used DFT calculations and crystallographic assessment of the N–S bond lengths to establish approximately 2*e* transfer to the SDI from the metal centres in titanocene and zirconocene complexes, **14**,[27] whilst a reductive insertion reaction of a zirconium nitride to an SDI has also been reported.[28] These discoveries of dramatic redox non-innocence accompanying such SDI complexes induced us to consider the degree of redox tuning that may be possible with variations in SDI substituents; however, there is an extreme paucity of reliable voltammetric data on SDIs in the literature.[29] We therefore set out to undertake a systematic study employing voltammetry, and here report a thorough comparative structural, spectroscopic, electrochemical, and EPR-spectroelectrochemical study on a deliberately selected series of 4- and 2,4,6-substituted diaryl SDIs (**1**–**9**, Figure 1). Their voltammetry is contrasted with that of the most studied SDIs in coordination chemistry, ^{t}Bu–NSN–^{t}Bu, **10**, and Me_3Si–NSN–$SiMe_3$, **11**.

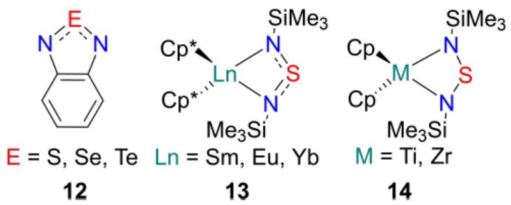

Figure 2. Line structures of some important compounds.

Results and Discussion

Synthesis

A series of nine aryl sulfur diimides (compounds **1**–**9**, Figure 1), with push- and pull ring substituents,[30] was synthesized, and the well-known *bis*-^{t}Bu, **10**, and *bis*-trimethylsilyl, **11**, analogues were also prepared by literature methods.[4a,31] Three synthetic routes were used for **1**–**9**, all beginning from the corresponding substituted aniline (Scheme 1). Method A proceeds by sulfinylation of the respective aniline by refluxing with thionyl chloride. Except for the case of *bis*(4-nitrophenyl)sulfur diimide (**7**), the sulfinylaniline is used in the next step without purification and reacted with potassium *tert*-butoxide to yield the sulfur diimide. Method A works for compounds **1**–**8** (compound **9** was not attempted by this method), but compounds **1**, **3**, and **4** were made in better yield by method B. Method B involves refluxing the substituted aniline with neat hexamethyldisilazane (HMDS) and an acid catalyst to produce a monosilylated aniline, which must be distilled before continuing. This is then reacted at

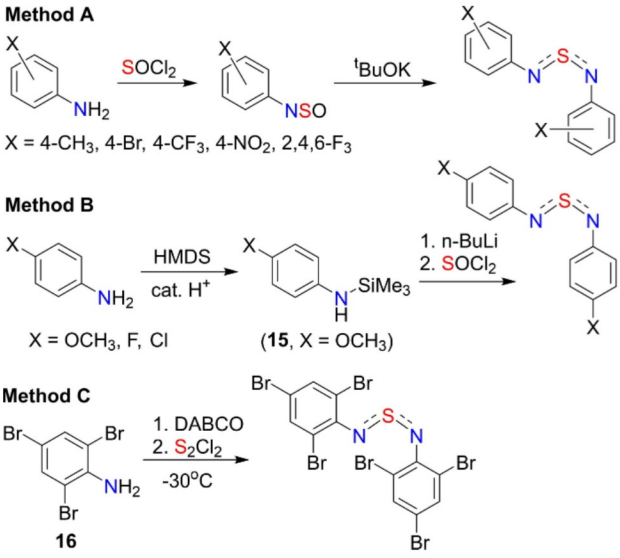

Scheme 1. Synthetic methods employed for the aryl SDIs (SDI compound labels identified in Figure 1).

−65 °C with an equimolar amount of butyllithium, followed by addition of thionyl chloride to yield the sulfur diimide. Compound **9** was synthesized using a one-step method adapted from Konstantinova et al.[32] in which the substituted aniline is reacted with sulfur monochloride in the presence of diazabicyclooctane (DABCO).

Compounds **1–5, 7**, and **9** are previously reported in the literature,[12–13] while compounds **6** and **8** are not, save for a failed attempt to synthesize **6**.[33] All have been fully characterized including with new single-crystal X-ray diffraction (SC-XRD) structures; the structures of reagents **15** and **16** were also determined (full details are in the Experimental and the Supporting Information).

Solid-State Structures from X-Ray Diffraction

Compounds **1–7** and **9** are all found to crystallize E/Z, and only **8** crystallizes as Z/Z (Figures 3 and 4, as well as Section 2 of the Supporting Information). In most cases, the Z-oriented phenyl ring is nearly coplanar to the NSN moiety, while the E-oriented ring is twisted out of plane to varying degrees. This is consistent with the other *para*-substituted aryl sulfur diimides in the CSD, namely refcodes BAZLOD,[34] NEMHIW,[33] and NEMHUI.[33] There is no clear correlation of the substituent's electron donating/withdrawing properties to the N–S–N–C_{ipso} torsion angles. This is well illustrated by the $Z'=2$ structure of **6** (see Figure 1), in which the E-oriented ring on N2 is almost co-planar to NSN (torsion angle 3.8(6)°), whereas that on N4 is strongly twisted (−48.3(5)°). While **9** crystallizes as E/Z, both phenyl rings are almost orthogonal, torsions of 85.9(3)° and 85.4(3)°, relative to the NSN moiety, presumably due to steric pressure from the large *ortho*-bromine substituents. This is a rare configuration, only otherwise observed in *bis*(2,4,6-*tri*-*tert*-butylphenyl)sulfurdiimide (CSD refcode: BEQHEK),[35] which also contains very bulky *ortho* substituents. Aside from these two cases, every example from the CSD of aryl SDIs with at least one *ortho* substituent crystallize as Z/Z, as does **8**.[13b,33, 35–36] Interestingly, the SC-XRD of **10**[37] (CSD refcode: HOVYAS01) and **11**[38] (YEFJUO) are found as E/Z.

Crystal structures of **2**, **3**, and **9** have been previously published with CSD refcodes: TOLIMS, NEMHUI,[33] and HEPZIL[13b] (the Cambridge Structure Database (CSD),[40] release 2023.2.0). Our redeterminations improve upon previous depositions, providing a full structure for TOLIMS, which only had unit cell information previously, and lower acquisition temperatures and R-factors for NEMHUI and HEPZIL. Further, all structure models presented in this work have been refined by a Hirshfeld

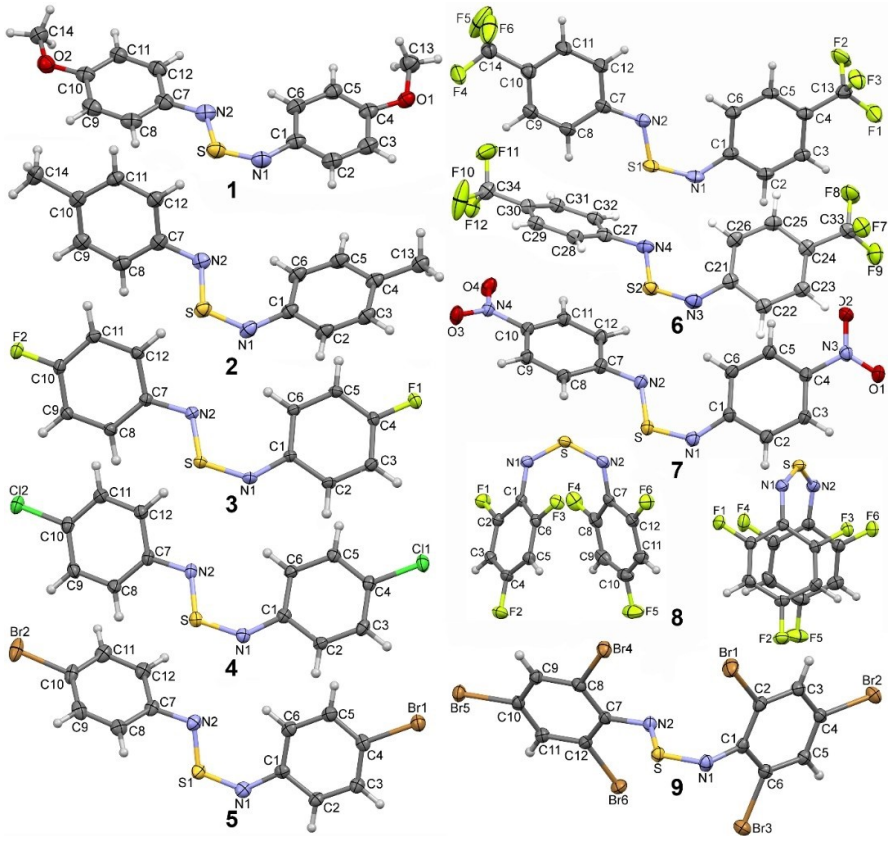

Figure 3. Displacement ellipsoids plots (40% probability) of **1–9** as found in the crystals. H atoms are rendered as spheres with 0.10 Å radii; full anisotropic rendering of H atoms via HAR for **1–9**, **15**, and **16** are provided in the Supporting Information (Figures S1–S11), as is the second molecule of the $Z'=2$ structure **5**; only the main component of CF_3 disorder in the structure of **6** is shown (see Figure S6).

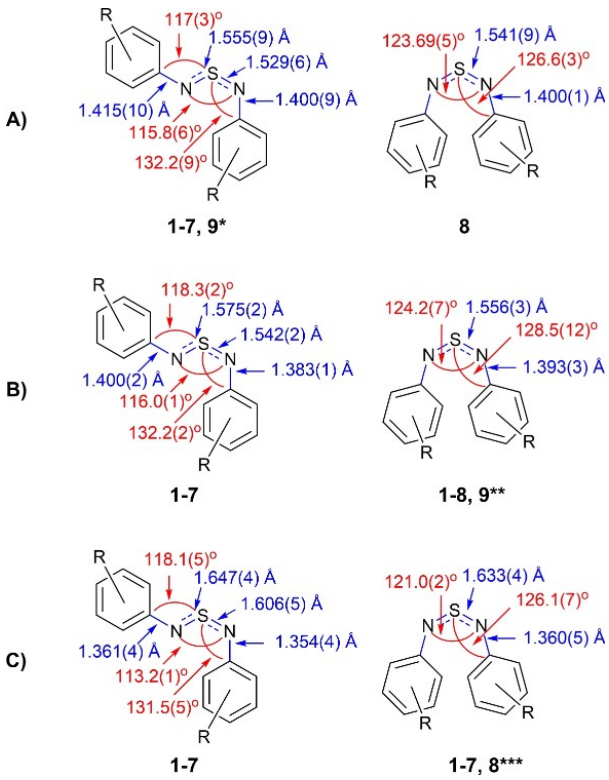

Figure 4. Averaged (A) experimental and (B) computed bond angles and bond lengths for neutral SDIs from SC-XRD structures in the E/Z and Z/Z conformations (at the RB3LYP-D3BJ/6-311++G(2d,p) level of theory). (C) Averaged computed geometries for the monoanions using UB3LYP-D3BJ/6-311++G(2d,p). Restrictions: * in (A), **1**–**7** and **9** are E/Z, but ∠SNC of the *Z* branch of **9** is an excluded outlier; ** in (B), both **8** and **9** are general outliers and excluded from E/Z, while in Z/Z the *d*(NS) of **9** are excluded outliers; *** in (C) likewise **8** and **9** are excluded from E/Z, whilst **9** is fully excluded from *Z/Z*, and the ∠NSN of **8** is excluded from Z/Z.

atom refinement (HAR) approach using the recently released NoSpherA2,[41] included with the current version of the Olex2 crystallographic software suite.[42] NoSpherA2 enables the use of custom atom scattering factors polarized to actual atom positions, enabling precise H-atom placement with near to neutron diffraction accuracy, and calculation of anisotropic displacement parameters for hydrogen atoms. Our group has previous experience applying NoSpherA2, demonstrating the remarkable improvement in bond precision over Independent Atom Model (IAM) refinement with relatively modest computational effort.[43] Accurate H-atom geometries are particularly important to this work because of the impact of dispersion interactions between the two R groups on each SDI on the geometries adopted. Further details on the refinement models adopted, along with a statistical analysis of structure precision improvements are provided in Section 3 and Table S27 of the Supporting Information for interested readers.

Full interatomic distances and angles are provided in the Supporting Information (Tables S2–S25). In view of the large number of structures, it was fortunate to discover that these data are generally very consistent. In Figure 4, geometric values that are averageable at the 99% confidence level are displayed. All the indicated parameters could be included in the averages for structures of **1**–**7**, which all crystallize as E/Z. Moreover, for **9**, though E/Z differs by the orthogonal displacement of the two aryl rings unlike the other seven cases, all the parameters *except* the S–N–C angle in the *Z* branch fit within the averages. The compilation of geometric data displayed in Figure 4(A) is the most systematic and reliable available for diaryl SDIs.

DFT Calculations

For each of the compounds **1**–**9**, density functional theory (DFT) calculations were performed on the neutral species. Geometry optimizations and frequency calculations were undertaken with multiple approaches, leading to the adoption of a triple-ζ Pople basis set with polarization functions to account for the electron rich NSN moiety; the well-attested B3LYP functional performed well. All three conformational isomers, E/E, E/Z, and Z/Z, were examined. The E/Z calculations compute with excellent geometric agreement with the solid-state structures obtained by SC-XRD for compounds **1**–**7**. (Figure 4B). For the computed neutral structures that are compiled in Figure 4(B), over both conformations, the average deviation magnitude is less than 1%. By contrast, the conformation computed with standard DFT methods for both **8** and **9** differ substantially from the XRD structures. **8** crystallizes in the Z/Z conformation, unlike all of the other sulfur diimides in this series, while **9** crystallizes E/Z, but in the optimized E/Z geometry, the *E*-oriented aryl ring approaches co-planarity with the NSN bridge, whereas in the experimental structure both aryl rings are nearly orthogonal to the NSN moiety. By making use of Grimme's post-SCF dispersion correction D3 (with Becke-Johnson damping),[44] the agreement between computational and experimental geometries became very close for all of **1** to **8** whilst the ring orientation in **9** remains different, possibly because co-planar or orthogonal $C_6H_2Br_3$ rings have a small energetic difference. Therefore, a relaxed scan DFT calculation was undertaken, showing that the barrier to rotation for the *E*-branch aryl ring is only 4 kJ/mol (see Section 4 of the Supporting Information). Fascinatingly, the computed Z/Z geometry is lower in energy than E/Z, with or without invoking the dispersion correction in the case of **8** and **9** (see Table 1 below).

Experimentally, the dominant solution state conformations of the *para*-substituted sulfur diimides (**1**–**7**) are proposed to be E/Z, while the dominant tri-substituted sulfur diimide conformations (**8**,**9**) are proposed to be Z/Z, based on the NMR and UV-vis evidence obtained in this work (see below) and by Zibarev and co-workers.[13b] This is a contrast to the solid-state conformation of **9**, known to be E/Z by crystallographic characterization. The calculated energies without empirical dispersion corrections conform to the proposed conformations, namely E/Z being the lowest energy conformation for **1**–**7**, and Z/Z the lowest energy conformation for **8** and **9** (Table 1). When dispersion correction is added, the lowest energy conformation for all of the sulfur diimides becomes Z/Z, reflecting a known tendency of D3BJ to overestimate (intramolecular) π-stacking

Table 1. Computed relative energies (kJ/mol) of **1–9** in neutral and monoanionic minimized geometries with and without empirical dispersion corrections applied.

		1	**2**	**3**	**4**	**5**	**6**	**7**	**8**	**9**	**10**	**11**
Substituent		4-OCH_3	4-CH_3	4-F	4-Cl	4-Br	4-CF_3	4-NO_2	2,4,6-F_3	2,4,6-Br_3	^{t}Bu	$SiMe_3$
Neutral D3BJ[a]	E/E	35.8	33.9	34.3	34.9	35.6	36.4	31.6	35.4	54.1	27.1	16.3
	E/Z	7.3	6.9	5.9	7.3	8.2	10.8	6.8	17.5	25.3	0.0	0.0
	Z/Z	0.0	0.0	0.0	0.0	0.0	0.0	0.0	0.0	0.0	30.3	11.9
Neutral No Disp[b]	E/E	25.1	23.8	25.2	24.3	24.1	22.4	21.6	13.3	20.5	22.1	10.3
	E/Z	0.0	0.0	0.0	0.0	0.0	0.0	0.0	0.3	4.7	0.0	0.0
	Z/Z	7.2	7.2	7.9	7.8	7.9	7.4	8.9	0.0	0.0	32.3	16.6
Anion D3BJ[c]	E/E	13.2	9.5	11.2	9.3	9.6	7.4	7.2	3.3	21.7	11.7	17.4
	E/Z	6.8	4.9	5.0	3.3	3.4	1.9	0.0	2.0	6.9	0.0	0.0
	Z/Z	0.0	0.0	0.0	0.0	0.0	0.0	4.7	0.0	0.0	[e]	[e]
Anion No Disp[d]	E/E	3.1	1.3	2.9	2.6	2.8	2.2	3.8	0.0	0.0	7.4	10.0
	E/Z	0.0	0.0	0.0	0.0	0.0	0.0	0.0	3.8	0.3	0.0	0.0
	Z/Z	5.4	7.0	6.6	8.1	8.6	10.0	16.3	15.8	15.4	[e]	[e]

[a] Employing the RB3LYP-D3BJ/6-311++G(2d,p) level of theory. [b] Employing the RB3LYP/6-311++G(2d,p) level of theory. [c] Employing the UB3LYP-D3BJ/6-311++G(2d,p) level of theory. [d] Employing the UB3LYP/6-311++G(2d,p) level of theory. [e] For both **10** and **11**, when the Z/Z structures are given a charge of −1, they spontaneously minimize to E/Z.

interactions between pendant aryl rings attached to thiazyls.[44–45] As there is convincing UV-vis and NMR evidence for compounds **1–7** being predominantly E/Z in solution, it seems likely that similar overestimation of π-stacking stabilization is operative for D3BJ correction in aryl SDIs.

Solution Structures from NMR

^{1}H, ^{13}C, and ^{19}F NMR data for **1–9** are presented in Table 2 and full archival spectra are provided in the Supporting Information (Figures S140–S182). The *para*-substituted aryl sulfur diimides, **1–7**, show fluxionality between the E/Z and Z/E conformations at ambient temperature, a phenomenon that was previously noted by a number of researchers in their analyses of the structure of sulfur diimides.[13b,38, 46] This is independently

Table 2. ^{1}H, [a,b,c] ^{13}C, [a,b,d] and ^{19}F [a,b,e] NMR data for **1–9** at ambient temperatures.[f]

Cmpd	H_2(X)[g]	H_3	X_4 (^{1}H, ^{19}F)	C_1	C_2	C_3	C_4	X_4(^{13}C)
1	6.75, d (8.3)	7.49, s	3.84, s	140.2, s	125.0, s	114.3, s	158.5, s	55.7, s
2	7.15, d (8.1)	7.37, d (7.2)	2.36, s	143.7, s	123.4, s	129.6, s	136.9, s	21.4, s
3	7.03, s	7.44, s	−113	142.1, d (1.9)	125.1, s	116.0, d (22.6)	161.3, d (248)	–
4	7.32, d (8.7)	7.41, d (7.8)	–	144.1, s	124.7, s	129.3, s	132.7, s	–
5	7.34, d (7.9)	7.47, d (8.6)	–	144.5, s	125.0, s	132.3, s	120.7, s	–
6	7.43, s	7.57, d (8.2)	−61.9	147.7, q (1.4)	123.2, s	126.4, q (3.7)	128.9, q (32.8)	124.1, q (272)
7	7.60, d (8.7)	8.27, d (9.0)	–	149.8, s	124.0, s	125.2, s	146.2, s	–
8	−113 (^{19}F)	6.52, m (abb'xx')	−109	117.9, td (17.7, 5.1)	153.6, ddd (252, 14.7, 7.0)	99.9, ddd (26.6, 23.6, 4.8)	160.3, dt (251, 14.4)	–
9	–	7.56, s	–	141.0, s	117.1, s	133.8, s	118.7, s	–

[a] In $CDCl_3$; format: δ (ppm), multiplicity, (J (Hz)). [b] Numbering scheme as in Figure 5, with H and X labelled as per the attached C atoms. [c] δ(^{1}H), relative to residual $CHCl_3$ at 7.27 ppm. [d] δ(^{13}C{^{1}H}), relative to residual $CHCl_3$ at 77.23 ppm. [e] δ(^{19}F{^{1}H}(**3**,**6**) or ^{19}F (**8**)), relative to external $CFCl_3$ at 0.00 ppm. [f] NMR data for **1–9** at low temperature is available in Table S30 in the Supporting Information. [g] All ^{1}H NMR signals for the *ortho*-H (H_1) of SDIs **1–7** are broad even at RT due to fluxionality.

evident both in the ^{1}H NMR from a significant broadening of the signals of the *ortho*-protons, and in ^{13}C NMR for the *ortho*-carbons. For example, the two doublets in the ^{1}H spectrum of **6** (Figure S160 in the SI) have highly disparate linewidths, with full widths at half maximum (FWHM) of 4.5 Hz and 22.0 Hz for the *meta* and *ortho* protons, respectively. Similarly, in the ^{13}C NMR of **3**, the *ortho* carbon signal is significantly broadened compared to the others, with FWHM = 91.6 Hz, compared to 13.1 Hz, 11.5 Hz, and 9.0 Hz for the *ipso*, *meta*, and *para* signals (Figure S150 in the SI). For compounds **1–7**, the order of the broadening effect in the ^{13}C NMR is $o > i > m > p$. Upon cooling to ~233 K, we observe splitting of some peaks into the distinct signals from the E and Z branches as the exchange is inhibited. The magnitude of this splitting follows the same order as above, $o > i > m > p$. Figure 5 is an overlay of ^{13}C{^{1}H} NMR spectra of compounds (a) **3** and (b) **9**, each taken at room temperature (RT) and −40 °C (295 K and 233 K) and truncated to highlight the aromatic regions (~100 ppm to ~170 ppm). Compound **3** was chosen as an exemplar of **1–7**, showing the fluxionality of the E/Z oriented SDIs by the splitting of *ipso*, *ortho*, and *meta* signals into separate peaks, one each for the E and Z branches of the SDI as the E/Z↔Z/E exchange is slowed by the reduced temperature. The spectrum of **9** was chosen to represent **8** and **9**, which are symmetrical, showing no splitting of peaks at reduced temperatures seen in **1–7**.

Zibarev et al. studied a series of aryl SDIs with bulky *ortho*-substituents, which included **9**, over a wide temperature range from 293 K to 163 K.[13b] They found that **9** contains exclusively one symmetrical conformer, while other SDIs with methyl groups in one or both *ortho* positions contained a mixture of 12%–16% unsymmetrical (E/Z) conformer. From NOE measurements of one of these compounds they were able to determine that the symmetrical geometry present was Z/Z, and not E/E. Independently, and around the same time, Herberhold et al. investigated a series of various alkyl SDIs, as well as phenyl SDI, and determined the conformation using ^{15}N NMR.[47] They used SDIs which are dominantly E/Z in geometry in solution, but contain a minor component of symmetrical conformer, and compared their ^{15}N NMR data of acyclic SDIs to that of several cyclic SDIs, which enforce a Z/Z geometry and provide an expected resonance for nitrogen. They found that the chemical shift of their symmetrical conformer was consistent with the cyclic SDIs, i.e. their symmetrical conformer was confirmed to be Z/Z. This issue is of particular importance for our study, since we wished to know what the dominant species were on which we perform the solution state voltammetry; fortunately we were able to use CH_2Cl_2 as the electrochemistry solvent, with expected isomer distributions similar to the $CDCl_3$ employed in the NMR studies.

A most helpful resource in assigning the ^{13}C NMR signals for all of the sulfur diimides was the table of aryl substituent effects on chemical shifts in Silverstein and Webster.[48] We used the established chemical shifts of diphenylsulfur diimide[49] to introduce new substituent parameters for R = NSN-Ar, enabling calculation of expected shifts for aryl SDIs (see Table S31 in the SI). Adding the modifiers from the table for the other substituents in each of our compounds resulted in excellent agreement with observed ^{13}C data for **1–7** (within 0.4 ppm), and good agreement with the more highly substituted **8** and **9** (within 2.5 ppm).

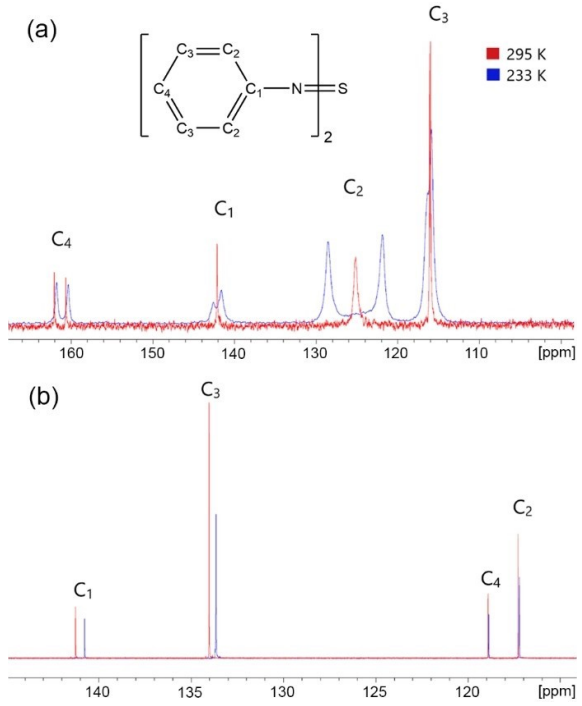

Figure 5. Overlay of ^{13}C{^{1}H} NMR spectra (aryl-C signals from ~110 to 165 ppm) at 295 and 233 K of (a) **3** and (b) **9**.

Electronic Structure and Bonding of SDIs

The previous section counters a persistent myth of SDIs – namely, that E/E should logically be the lowest energy conformation[50] – and we now turn to a second wrong idea, that the (genuinely very short) S–N bonds are simultaneous 'double bonds' to hypervalent sulfur. Previous work, particularly of Stalke and co-workers, has provided irrefutable experimental and computational evidence against this idea,[11] brilliantly confirming that the Lewis resonance formulation (Figure 1) is fully valid, whilst also elucidating the real differences in structures and reactivity that result from an allylic resonance with a third-period central atom. This situation is notably different from other heteroallylic systems, such as phospha(III)amidines and diphospha(III)amidines, wherein the central atom remains C.[51] Hence, there is not only sulfur diimide, but also an extensive triimide chemistry.[6a,b,52] Although Pauling is strongly associated with the now-deprecated notion of valence expansion by hybridization (i.e. dsp^3 models for S^{IV}),[53] it seems to be forgotten that his even more fundamental concept of element electronegativity was directly based on the concept of enhanced strengths of bonds with partial ionic character.[54] This recognition leads directly to the idea of bond shortening from an ionic contribution to a covalent bond,

which Leusser *et al.* conclude causes the foreshortened bonds in SDIs.[11b] It is a fundamental property of thiazyl chemistry that SN π-bonds are highly polarized.[55]

Despite intensive computational investigations over two decades,[50,56] the literature is remarkably devoid of a thorough discussion of the electronic structures of SDIs, which not only display allylic-type resonance but are exceedingly electron rich from the four formally non-bonded electron pairs.In our analysis (Figure 6), we restrict the discussion to just the E/Z and Z/Z isomers that can be ground state geometries (though the situation in E/E will be very similar), and we commence by formally treating the parent HNSNH molecules before considering the influences of aryl substituents. Importantly, the parent SDI also serves as model system for **10** and **11**. Figure 6 presents the computed energy levels and Kohn-Sham MO surfaces, omitting the four lowest levels that correspond to the σ-bonds (i.e. primarily constituted from the N and S atomic *s* orbitals). This leaves the filled and virtual orbitals that have formal π-symmetry as well as *n*(S) and *n*(N), i.e. the MOs associated with "lone pair" character. The scenarios for the two isomers are very similar, though at this level of theory, the sequence of the *n*1 and π1 MOs is reversed (due to a 0.72 eV stabilization of the former in E/Z). There is considerable mixing of the *n*(S) and *n*(N) levels in E/Z, enabled by the symmetry lowering from C_{2v} to C_s. The net NS bond order is easily rationalized as 1.5 from the four σ bonds, non-bonding *n1*–*n*3, plus double occupancy of π1 (bonding) and π2 (non-bonding) in both isomers (compare computed natural bonding orbitals theory, NBO, estimates of 1.33 for the *Z* branch and 1.40 for *E* in the E/Z isomer,[11b] or Wiberg bond index, reported as a single value of 1.54, without clarifying if this is an average or taken from a symmetric isomer).[56m] There are just two experimental reports on this parent SDI. Carlsen et al. prepared HNSNH in the gas phase by pyrolysis of tetrasulfur tetraimide, $S_4(NH)_4$[57] and identified it from mass spectrometry and ultra-violet photoelectron spectroscopy (UV-PES), but the PE spectrum has unfortunately not been reported.[57] Haas prepared and then isolated HNSNH in a frozen Ar matrix, where it was identified as a mixture of E/Z and Z/Z by infrared spectroscopy (see below). Previous computational studies on HNSNH have been reported by Zahedi,[50] Shahbazian,[56k] and Tuononen[56g] but only

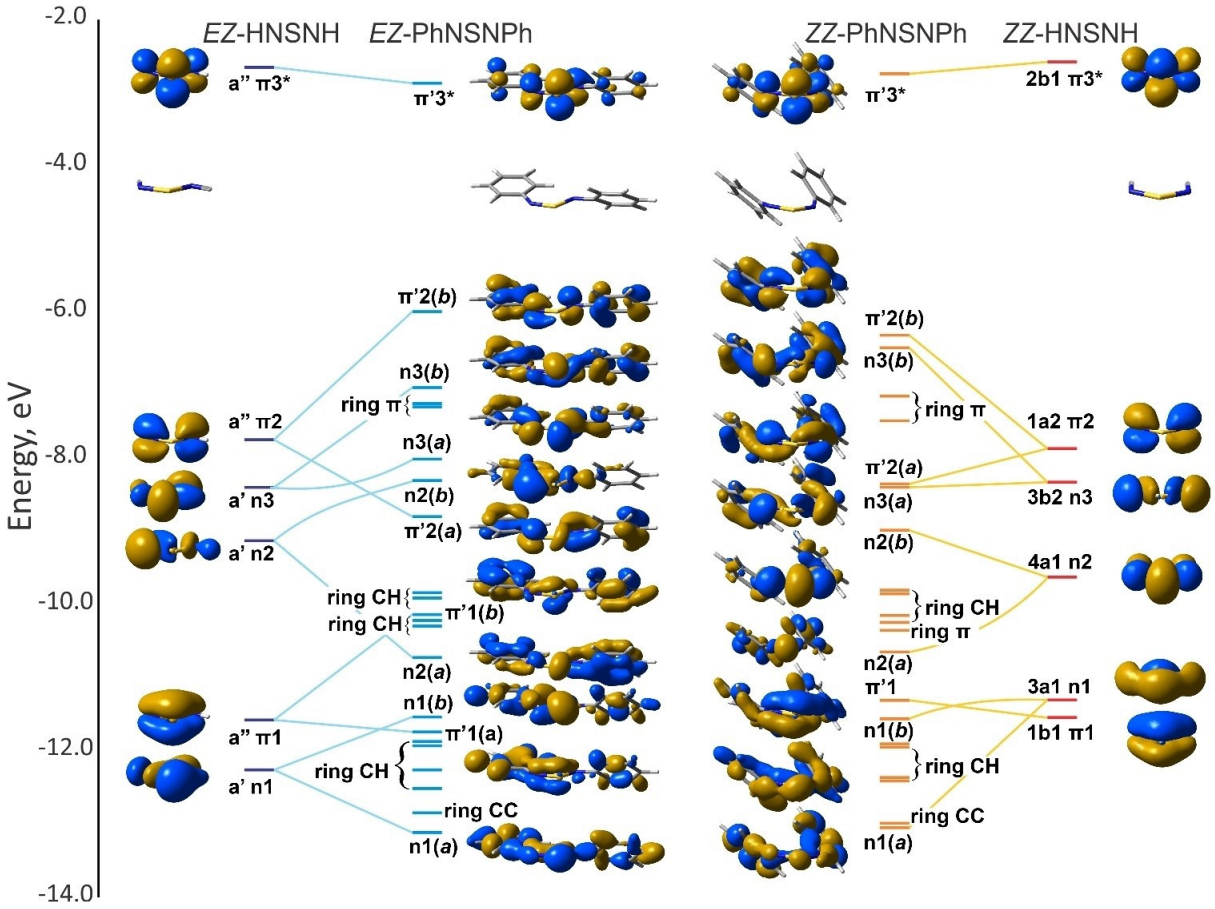

Figure 6. Molecular orbital correlation diagram comparing the valence π and lone pair (LP) energy levels, with Kohn-Sham orbital surfaces (isovalues = 0.04), of the parent HNSNH and the diphenyl SDI, as computed at the B3LYP-D3BJ/6-311G++(2d,p) level of theory. The E/Z and Z/Z isomers in their gas-phase lowest energy conformations are shown. The molecular orientations of the MO surfaces as well as the first virtual levels are shown at top. Energy levels for the parent SDIs are doubly labelled by symmetry and type.

structure and isomer preferences were discussed and no details on molecular orbitals or bonding have been published.

For each isomer, approximate correlations are provided to corresponding energy levels in the PhNSNPh cases, which are used here as simplified models for **1–9**. Recognize first the complete loss of symmetry, in both instances, due to out of plane aryl rotation; hence there is no longer a formal σ/π distinction, though the orbitals designated as π′ are those with the greatest π character over the planar NSN region; moreover, rapid N–C_{ipso} rotation in solution may render the SDIs effectively planar. The influence of the aryl groups is extremely strong and in almost all cases the parent levels are recognized in one significantly stabilized and one strongly destabilized aryl-interacting MO (respectively designated by the *a* and *b* distinctions in the labels of Figure 6).[56a] The frontier molecular orbitals (FMOs) are still recognizable in π′2 and π′3, for both isomers, but especially for the former, the aryl contributions are very significant, resulting in a strong destabilization of the HOMO. This results in a much smaller HOMO-LUMO gap for the aryl systems (with significant impacts on colour and hence UV-vis spectroscopy, see below). The correlation lines drawn in Figure 6 are only approximate due to the evident σ/π mixing; MO surfaces and lines are drawn only for those of the PhNSNPh energy levels with significant NSN contributions, whereas those that are not drawn are strongly localized on the aromatic rings. This is especially so for the HOMO-1 and HOMO-2 'ring π' MOs, which have negligible impact on bonding but are very much in play for electronic excitation transitions (see below). In summary, aryl SDIs have complex electronic structures with many highly-polarizable *p*(π) contributions as well as six (formally) σ non-bonding electrons. Additionally, the obvious flexibility of the chain structures and NMR evidence for fluxionality in solution are expected to greatly complicate their real-world electronic structures. And yet, despite all the additional complexity, the FMOs will still have the expected sequence of $(n3)^2(\pi2)^2(\pi3)^0$ levels across the substituent classes being considered in this work, consistent with the line drawings of e.g. Figure 1. Reactivity towards either nucleophiles[6,58] or free electrons[56d] is expected at the π3/π′3 LUMOs, for which the highest coefficients are always at sulfur. At the same time, significant delocalization of both the HOMO and LUMO into the aryl π-system will influence the redox tuning that is the topic of this work. Excellent agreement is found between the energy levels for the E/Z isomer of PhNSNPh in our calculations (via Koopman's theorem) with an experimental investigation by UV-PES.[14]

Infrared Spectroscopy

The original literature assignments, dating from their first syntheses, were based on analogies to organo-nitrogen analogues including PhNSO.[5,12,32,59] Several independent groups assigned the various NSN vibrational modes to different bands.[12,32,59a] The application of vibrational energy calculations from modern, dispersion corrected, DFT methods paints a picture with significant differences. There is to our knowledge only a single published study presenting the vibrational spectra of the parent HNSNH (Table 3).[60] The data are reported in a frozen Ar matrix and these compounds were produced as mixtures from trapping reactions, present as E/Z and Z/Z isomer mixtures as expected from miniscule differences in their energies.[56k,60] Excellent agreement of an average of $\pm 10\ cm^{-1}$ is achieved between these experimental values and our B3LYP-D3BJ/6-311++G(2d,p) DFT calculations, and with good agreement on intensities, leading to a very high confidence in the assignments of the spectral bands. The relevant NSN vibrations (3 for E/Z and 2 for Z/Z, reflecting C_s and C_{2v} point group symmetries, respectively) are included in Table 3 and a full assignment is presented in Table S44. To further calibrate our DFT computed spectra, we also undertook a full geometry minimization with frequency assignments for *Z*-PhNSO since it has been most often used to predict the bands in aryl SDIs. Our approach substantiates the original assignments of Meij et al. for the natural and ^{15}N enriched compounds in IR and Raman[59c] and the agreement of computed with experimental values averages to $\pm 12\ cm^{-1}$ (Table S45).

The same approach, when applied to PhNSNPh, for which complete IR data is available in the literature,[5] along with $^{14}N/^{15}N$ comparisons for both IR and Raman for some of the principal bands,[59c] achieved similar agreement levels ($\pm 10\ cm^{-1}$), but with a considerably more complex interpretation (see Table S46). In short, the assumption that frequency assignments from the terminal PhNSO molecule could be directly applied to the disubstituted PhNSNPh was, in retrospect, incorrect. This, along with the very strong mixing of vibrational modes of the phenyl ring atoms and those of the bridging –NSN– moiety, casts doubt on the assignment of the $1268\ cm^{-1}$ band to ν_{as}(NSN).[5,59c] There are in fact three very close, strong bands (1298, 1265 and $1218\ cm^{-1}$), whose assignment is now identified to (very similar) vibrations with mixed character, namely: the *Z*-branch ν_{as}(ringNS), ν_{as}(ringNSring), and the *E*-branch ν_{as}(ringNS). The ν_{as}(NSN) vibrational mode therefore appears to be distributed amongst these three bands and that at $1070\ cm^{-1}$, of which the latter is more concentrated on the NSN atoms and should be considered as the primary ν_{as}(NSN) band in diaryl SDIs. Interestingly, the energies of these four bands bracket those of the fundamental in HNSNH at $1181\ cm^{-1}$. By contrast, the symmetric stretch, ν_s(NSN), in PhNSNPh at $957\ cm^{-1}$ is much closer to the fundamental at $934\ cm^{-1}$ in HNSNH, suggesting that this mode is far less susceptible to mixing with the aryl ring vibrations. Fascinatingly, the symmetric bend, δ_s(NSN), at $803\ cm^{-1}$ in PhNSNPh is double the energy of the fundamental at $410\ cm^{-1}$ in HNSNH. We do not have an explanation for this phenomenon.

The exceptional opportunity afforded in this work, that of having nine further aryl SDIs for which the solid-state geometries have been unambiguously determined by crystallographic analysis, has now enabled us to confidently assign the key vibrational frequencies of these crystalline solids, as presented in Table 3, each based on computed spectra from DFT calculations. Despite this, we have not utilized FTIR further in our investigation of SDI conformations, since the computed signals for the E/E, E/Z, and Z/Z conformations, typically

Table 3. Experimental and computed IR data for HNSNH and aryl SDIs.[a]

Code	Subst.	ν(ringNS)	ν(rNSNr)	ν(ringNS)	ν_{as}(NSN)	ν_{s}(NSN)	δ(NSN)	δ(NSN)	ρ(NSN)
	H (E/Z)[b]	n/a	n/a	n/a	1181 s *1166, 13%*	934 m *935, 11%*	410 w *416, 17%*	n/a	n/a
	H (Z/Z)[b]	n/a	n/a	n/a	1157 m *1121, 65%*	unobs. *907, 9%*	410 w *412, 17%*	n/a	n/a
	Ph[c]	1298 s[d] *1293, 46%*	1265 s *1258, 98%*	1218 s[e] *1216, 100%*	1070 s *1050, 83%*	957 m *943, 24%*	803 m *790, 21%*	634 s *631, 21%*	337 w *333, 5%*
1	4-OCH_3	1268 m *1272, 5%*	1239 m *1230, 100%*	Unobs.[g] *1214, 27%*	1027 vs *1044, 41%*	952 vs *936, 4%*	743 s *740, 1%*	585 s *584, 9%*	417 w *411, 1%*
2	4-CH_3	1293 m[d] *1294, 30%*	1263 m *1256, 95%*	1223 m[e] *1218, 97%*	1062 s *1043, 81%*	961 m *942, 27%*	750 m *739, 21%*	585 w *580, 13%*	386 m *383, 10%*
3	4-F	1306 w *1297, 5%*	1270 m *1258, 10%*	1206 vs *1200, 92%*[h]	1061 s *1043, 28%*	958 *943, 12%*	759 m *747, 4%*	581 s *577, 14%*	410 s *411, 1%*
4	4-Cl	1294 m[d] *1293, 26%*	1268 s *1252, 33%*	1219 m[e] *1219, 50%*	1061 s *1041, 62%*	967 m *943, 13%*	815 vs *790, 11%*	683 m *676 5%*	389 vs *386, 41%*
5	4-Br	1293 w[d] *1292, 8%*	1267 m *1252, 36%*	1221 m[e] *1220, 31%*	1058 s *1039, 41%*	957 m *929, 5%*	799 s *787, 24%*	666 m *657, 5%*	382 s *376, 5%*
6	4-CF_3	1318 vs[d] *1307, 18%*	1273 s *1260, 61%*	1236 m[e] *1224, 33%*	1049 vs *1033, 55%*	967 m *949, 5%*	717 w *725, 3%*	654 m *651, 1%*	436 w *429, <1%*
7	4-NO_2	1252 vs[d] *1264, 71%*	1314 vs[f] *1318, 100%*	1232 sh[e] *1225, 44%*	1059 m *1045, 16%*	967 w *945, 4%*	787 m *784, 8%*	676 m *666, 2%*	389 m *363, 1%*
8	2,4,6-F_3	1443 vs[i] *1447, 68%*	1250 sh[i] *1252, 66%*	1240 sh[i] *1243, 4%*	1038 vs *1047, 42%*	985 vs *972, 23%*	748 m *754, 4%*	689 s *682, 18%*	438 s *423. 5%*
9	2,4,6-Br_3	1248 s[d] *1234, 97%*	1422 vs[f] *1396, 52%*	1240 s[e] *1228, 16%*	1093 m *1069, 44%*	987 w *978, 16%*	820 m *799, 25%*	675 m *654, 15%*	560 s *560, 6%*

[a] Data from this work unless noted, from crystalline solid using ATR/KBr; the second line of each entry are the computed values, at the B3LYP-D3BJ/6-311++G(2d,p) level of theory in Gaussian W16. [b] Data from Haas et al.;[60] frozen Ar matrix. [c] Data from Cramer,[5] or Meij et al.[59c] Liquid thin films. [d] *Z* branch only. [e] *E* branch only. [f] ν(rNSNr) contribution; there are six ring breathing bands that strongly couple to the NO_2 groups and weakly to NSN. Very weak [g] Obscured by very large ν(ring) band, 1239 cm^{-1}. [h] strongly coupled to C–F vibration, splits E and Z. [i] The 1287 s band (computed 1266, 58%) found at the more normal energy does not have NSN character; this is instead merged into one of three high energy bands that merge with ν(ring-Br). [j] In Z/Z there is C_2 symmetry; two of these bands have ν(rNSNr) character, as and s, and overlay a strong ν(C–F) at 1265 cm^{-1}.

differing by a few tens of wavenumbers (see Figures S104–S139 in the Supporting Information), are probably too similar to reliably identify specific isomers or mixtures in solution.

Mechanisms of SDI Isomer Interconversion

In a 1983-era computational study employing rigid scan methods, Raghavachari et al. proposed an isomerism mechanism for the parent SDI, HNSNH, that is intermediate between N–S bond rotation and in-plane inversion.[61] Later, Zahedi et al. applied QST2 and QST3 methods to search for transition states for dimethyl sulfur diimide.[56h] They concluded that the interconversion paths only exist between E/Z↔E/E and E/Z↔Z/Z, reporting transition state energies ranging from +47 to +88 kJ/mol relative to the isomer energies. However, little information was provided on the mechanism(s) of interconversion. We applied modern relaxed scan DFT calculations, using our standard B3LYP-D3BJ/6-311++G(2d,p) level of theory, for interconverting HNSNH along the paths proposed by Zahedi. Indeed, for this compound, the lowest computed path between isomers is effectively N–S bond rotation with only minor departures from planarity at the N atoms (see Section 4 of the Supporting Information). The transition states (TS) are confirmed to be saddle points (one imaginary frequency) and the paths have been confirmed by intrinsic reaction coordinate (IRC) calculations, conducted forward and backwards from the TS.[62] Also in agreement is that the energies are in the order Z/Z < E/Z (+0.7) < E/E (+13.9 kJ/mol). The computed barriers between Z/Z to E/Z (+68), and E/Z to E/E (+77 kJ/mol) along the relaxed scans are quite similar to what Raghavachari reported.

However, while similar transition states could be found for interconversions of PhNSNPh, employed as a model system for **1–9**, it was found that the S–N–C_{ipso} angles open up considerably (to ~150°). Moreover, IRC scans detect very different paths over the barriers (Figure 7). After opening these angles, a subtle re-organization involving inversion at one or both N atoms occurs that requires little further changes in the aryl ring orientations, consistent with the principle of least nuclear motion (PLNM).[63] Figure 7 shows a few key geometries through the Z/Z↔E/Z IRC path and some moving images (as .gif files) are also provided with the Supporting Information, to aid in visualization. The key point is that the aryl SDIs, possibly as a result of resonance delocalization into the aromatic rings, have access to surprisingly low energy paths between isomers. The computed barrier energies are +54 kJ/mol for E/Z↔Z/Z and +78 kJ/mol for E/Z↔E/E. These barrier energies are consistent

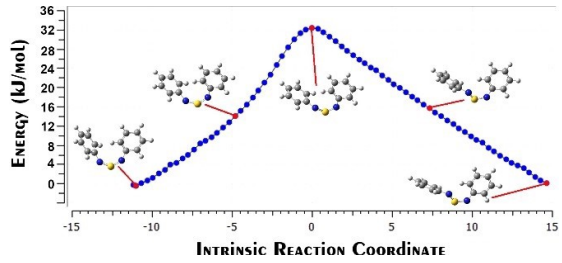

Figure 7. B3LYP-D3BJ/6-311++G(2d,p) calculation of IRC path for conversion of PhNSNPh from Z/Z (left) to Z/E (right); as is common for this type of calculation, the barrier shown is not the full height because the start and end points are not fully optimized in the IRC calculations.

with the E/Z↔Z/E fluxionality established by solution NMR for **1–7** at RT. Moreover, the slightly higher barriers to, and considerably higher energies computed for E/E, are consistent with a very low population but easy access to this conformer when required (as in chelation to metals).

UV-vis and TD-DFT

The UV-vis absorption spectra of the intensely coloured aryl SDIs **1–9** were measured as solutions in CH_2Cl_2 (Figure 8a).[64] These are strong chromophores, with absorption coefficients ranging from 3600 (**9**) to almost 15000 $L \cdot mol^{-1} \cdot cm^{-1}$ (**1**). Of particular interest to this study was the observation of distinct variations in the principal absorption maxima, λ_1 and λ_2, in the visible region. The *para*-substituted aryl SDIs **1–7** band maxima are more intense ($\varepsilon_{max} > 5000$) and the order of intensities is $\lambda_1 > \lambda_2$, whereas the bands for **8**, **9** feature $\lambda_1 < \lambda_2$ and the maximum intensities are lower ($\varepsilon_{max} < 5000$). There are significant variations in the positions of the band maxima, which generally follow the electron withdrawing propensities of the substituents, but not fully. The band envelope differences suggested that potentially the major components in solution may be different for these two sets of compounds (as already suspected from the NMR evidence). Hence, we studied predicted absorption spectra using TD-DFT calculations with the optimized isomer structures.

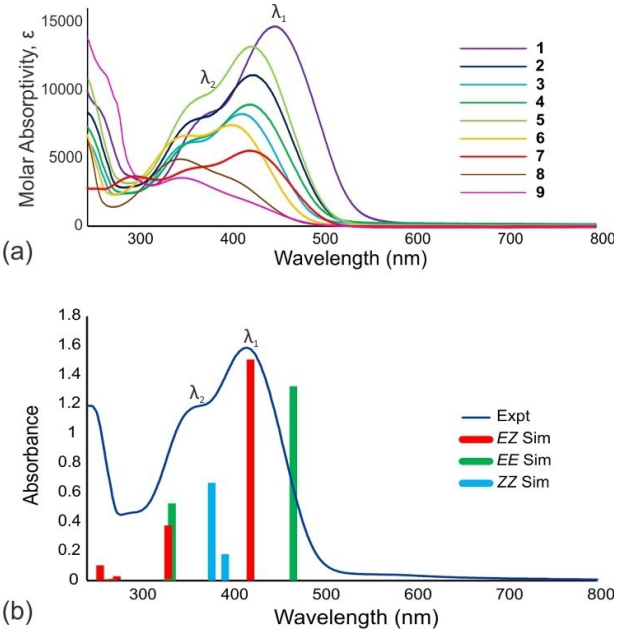

Figure 8. (a) Overlaid spectral traces in the visible and near-UV region for **1–9** as measured in dilute CH_2Cl_2 solutions (10 mm pathlength quartz cells). (b) UV-vis spectrum of **3** (blue trace) with calculated oscillators from TD-DFT frequency calculations of the possible conformers (E/E = Green, E/Z = Red, Z/Z = Light Blue).

Single point TD-DFT calculations were performed on compounds **1–9** using CAMB3LYP-D3BJ/6-311++G(2d,p) and a PCM model of solvation for CH_2Cl_2. N = 6 singlet states were solved for **1–8**, and N = 12 singlet states were solved for **9**. Calculations were run for all conformations (E/E, E/Z, Z/Z), which showed that the closest agreement between simulation and experiment was achieved with the proposed solution state conformations, namely E/Z for the *para*-substituted compounds **1–7**, and Z/Z for the tri-substituted compounds **8** and **9** (Table 4 and Figures S95 to S103), in accord with our DFT and NMR results (Table 1 and Figure 5b). While this method will be insensitive to minor isomers, it has great and heretofore untapped utility in assigning the principal conformation of SDIs in solution.

The computed oscillators for each of the three possible conformations are sufficiently distinct to enable confident assignment of the experimental spectra as containing predominantly E/Z or Z/Z conformers of the SDI. The calculated values for **8** closely conform to experimental values, while the calculated values for **9** see a higher deviation from experimental, most likely because of the known over-estimation of stabilization due to intramolecular π-stacking introduced by the D3BJ dispersion correction. Notwithstanding, even the largest deviations of the simulated UV-vis oscillators fit sufficiently well to the experimental spectra, and this simulated set of data is strongly supportive of our proposed compositions of the sulfur diimides in solution. It may be noted that Sicinska et al. previously assigned the two bands in these spectra to individual isomers, an assumption that can now be shown to have been correct in some cases, for example by the identifications shown in Figure 8(b).[46c]

Voltammetry

The electrochemical properties of the sulfur diimides were assessed by square wave (SWV) and cyclic voltammetry (CV) using the CH_2Cl_2/0.4 M [$^nBu_4$][PF_6] solvent-electrolyte combination uniformly. The electrochemical processes by CV for each sulfur diimide were shown to be under diffusion control by a linear plot of peak currents versus the square root of scan rates (Figures S64–S72 in Supporting Information). All samples were referenced internally to the ferrocene/ferrocenium redox process (designated in this work by $Fc^{+/0}$) at 0.0 V.[65] Key voltammetric data for **1–11** are reported in Table 5 in CH_2Cl_2 at a scan

Table 4. Experimental vs. TD-DFT principal peaks from UV-vis measurements and calculations.

		Experimental (nm)		TD-DFT (nm)[a]		Difference (nm)	
Comp.	Subst.	λ1	λ2	λ1	λ2	λ1	λ2
1[b]	4-OCH_3	453.1	382.9	456.5	339.8	3.4	43.1
2[b]	4-CH_3	431.0	370.8	433.1	336.5	2.1	34.3
3[b]	4-F	418.3	360.9	421.7	331.9	3.4	29.0
4[b]	4-Cl	427.0	367.3	429.6	336.7	2.6	30.6
5[b]	4-Br	427.9	372.1	430.6	337.6	2.7	34.5
6[b]	4-CF_3	406.2	355.9	409.9	334.9	3.7	21.0
7[b]	4-NO_2	425.9	372.1	432.2	345.4	6.3	26.7
8[c,d]	2,4,6-F_3	407	350.1	401.1	353.2	6	3.1
9[c,d]	2,4,6-Br_3	428	353.4	412.8	333.8	15	19.6
					Average	5.0	26.9
					Std. Dev.	3.9	10.8

[a] TD-DFT calculations used CAMB3LYP-D3BJ/6-311++G(2d,p), with CH_2Cl_2 PCM solvation model. [b] TD-DFT values given are calculated oscillators for the E/Z conformation of the SDI. [c] TD-DFT values given are calculated oscillators for the Z/Z conformation of the SDI. [d] λ_1 values for **8** and **9** are estimated due to poorly defined peaks.

Table 5. Summary of cyclic and square wave voltammetric data for redox processes of **1**–**11**.[a]

Process:	−1/−2			0/−1						+1/0	
Compd.	E_p^{c2} (V)	E_{SW}^2 (V)	$\Delta E_p^{c(1-2)}$	E_p^{c1} (V)	E_p^{a1} (V)	E_m^1 (V)	ΔE_{pp} (V)	I_a/I_c [b]	E_{SW}^1 (V)	E_p^{a3} (V)	$\Delta E_p^{a(3-1)}$
1	−2.131	−2.034	0.414	−1.717	−1.589	−1.653	0.128	0.52	−1.642	0.749	2.338
2	−2.036	−1.966	0.391	−1.645	−1.527	−1.586	0.118	0.64	−1.566	1.081	2.608
3	−1.987	−2.047	0.391	−1.596	−1.453	−1.525	0.143	0.65	−1.547	1.209	2.662
4	−1.871	−1.765	0.404	−1.467	−1.335	−1.401	0.132	0.67	−1.394	1.229	2.564
5	−1.889	−1.917	0.430	−1.459	−1.330	−1.395	0.129	0.73	−1.408	1.247	2.577
6	−1.720	−1.653	0.407	−1.313	−1.175	−1.244	0.138	0.70	−1.254	0.969[c]	2.144
7	−1.871	−1.793	0.886	−0.985	−0.863	−0.924	0.122	0.83	−0.912	1.109[d]	1.972
8	−2.157	−2.064	0.678	−1.479	−1.279	−1.379	0.200	1.00	−1.404	–	–
9	−1.721	−1.706	0.319	−1.402	−1.255	−1.328	0.147	0.64	−1.334	1.143	2.398
10	–	–	–	−2.571	–	–	–	–	−2.627	–	–
11	–	–	–	−2.717	–	–	–	–	−2.347	–	–

[a] GC electrode, A = 7.1 mm^2, ν = 0.2 $V s^{-1}$, T = 22 °C, with 0.4 M [^{n}Bu_4N][PF_6] supporting electrolyte in CH_2Cl_2. All potentials are Volts vs E^0 $Fc^{+/0}$. [b] I_a/I_c ratios are estimated except for **3**, **7**, and **8**, due to unsatisfactory baseline for anodic component (−/2- process disrupted baseline for all other compounds). [c] A second and more intense oxidation peak at 1.55 V is observed, with a better fitting $\Delta E_p^{a(3-1)}$ of 2.72 V. [d] A second and more intense oxidation peak at 1.74 V is observed, with a better fitting $\Delta E_p^{a(3-1)}$ of 2.60 V.

rate of 0.2 $V \cdot s^{-1}$ and more detailed data are provided in the Supporting Information (Tables S32A–S33) along with exhaustive SWV and CV plots (Figures S18–S63). The voltammetric responses for the nine aryl SDIs are broadly comparable but shift significantly over the accessible solvent/electrolyte window (Table 5 and Supporting Information), whereas **10** and **11** each show only one irreversible reduction process at very negative potentials.[25]

Typically, the aryl SDIs **1** to **9** show three processes (Figure 9), namely a first (labelled E^1) and second (E^2) reduction and an oxidation (E^3, not reported for **8** because ill defined). Importantly, E^1 has been shown to be a one-electron process, in all cases, by simultaneous electrochemical electron paramagnetic resonance (SEEPR) spectroscopy (see below for details) through the generation of radical anions *in situ* at the specified potentials. By comparison of the peak currents, E^3 is readily confirmed to also be a 1*e* transfer in the oxidation of **1**, for which the oxidation is well behaved with a strong return wave. A wide range of potentials is displayed with differing substituents (Figure 10), affecting both the cathodic and anodic processes, with a variation in E_m^1 from −0.92 to −1.65 V. As shown, E^1 is much more negative for **1** than for **6**. Similarly, E^3 is found much more positive in **6** than in **1**, and the difference may be even larger than indicated as there is some uncertainty in the correct oxidation peak assignments of **6**–**9**. However, as all attempts to confirm the identity for E^3 by SEEPR have thus far failed, detailed analysis will be restricted to E^1.

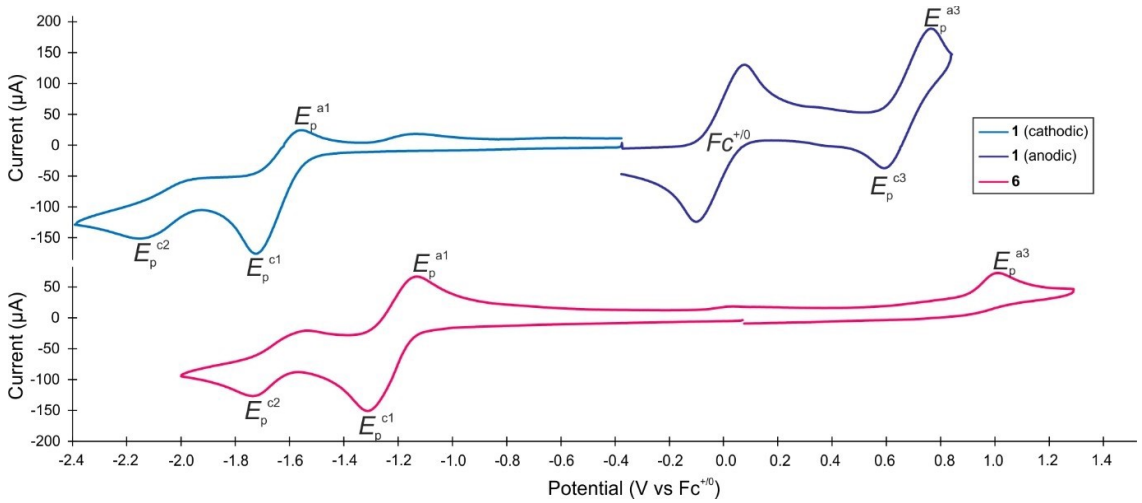

Figure 9. Comparative CV scans illustrating the most accessible redox processes in the anodic and cathodic regimes for representative examples of electron donating (top, **1**) contrasted with electron withdrawing (bottom, **6**) aryl SDIs. The top anodic trace also shows the signal from the ferrocene internal standard that is added to the analyte/electrolyte solutions in final scans. Initial scan directions are cathodic for **1** (cathodic) and **6**; anodic for **1** (anodic).

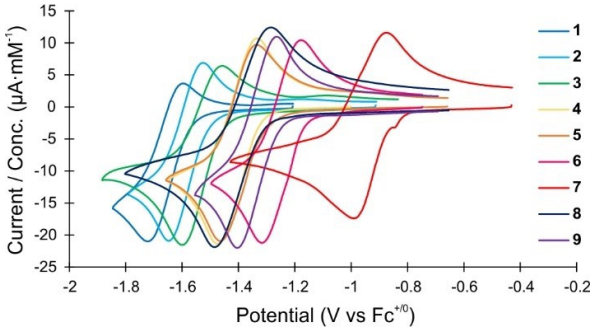

Figure 10. Overlays of cyclic voltammograms of the 0/- process for compounds **1–9**, referenced to $Fc^{+/0}$ at 0.0 V; initial scan directions are cathodic. The y-axis values are scaled to the experimental concentration of each species to present a relatively uniform set of overlaid cyclic voltammograms. A similar overlay of CVs without adjustment for concentration is found in Figure S18 in the Supporting Information.

The redox stability window $\Delta E_p^{a(3-1)}$ for all the aryl SDIs is large (average of 2.41 V), fairly constant and not apparently correlating with any other feature of the data (see below). The redox window $\Delta E_p^{c(1-2)}$, ranging from 0.32 to 0.89 V is small for all but the most electron withdrawing substituents (NO_2 in **7** and 2,4,6-trifluorophenyl in **8**). Significantly, in **7** the E^2 process shows a strong return wave and peak currents very comparable to those of E^1, thus consistent with a second 1*e* reduction. The E^2 peak currents for all the other aryl SDIs are anomalously small, which also needs further discussion (to follow). Formal potentials, measured as E^1_m, could only be obtained for the first reduction; remaining processes and determinations of averages and ranges employ the relevant cathodic or anodic peak potentials.

A clear pattern (as illustrated in Figure 10) emerges from the voltammograms that the more electron withdrawing substituents correspond to less negative E^1 potentials, and the more electron donating substituents correspond to more negative E^1. Since the LUMO topologies identified in DFT calculations in aryl SDIs of both E/Z and Z/Z conformations have significant coefficients at aromatic ring C atoms (Figures 6 and S73), these trends fit with the determined electronic structures. Indeed, the magnitude of the substituent effect in **1–9** on E^1 processes is remarkably large, with a 0.73 V difference between the most electron donating and electron withdrawing substituents. The magnitude of the substituent effects in aryl sulfur diimides is even greater than one of the most important ligands in redox non-innocent ligand research, 2,2′-bipyridine, which shows a range of only 0.59 V with the same substituents as this sulfur diimide series, in a 4,4′-X_2-2,2′-bipy configuration.[66] A contrasting class of comparators are aryl-1,2,3,5-dithiadiazoles (DTDA), which share with SDIs the characteristic of redox MOs centred on delocalized SN bonds. The reductions of these neutral radical species are much less sensitive to remote substituent effects, showing a range of just 0.12 V between 4-methoxy and 4-trifluoromethyl aryl substituents, compared to 0.41 V for sulfur diimides.[30c] This has been attributed to a node in the SOMO of DTDA between the phenyl ring and the heterocycle, which effectively insulates the electronic environment of the heterocycle from the resonance effects of the aryl substituents.

An additional issue highlighted in the series of overlapping E^1 CV traces shown in Figure 10 is the significance of the marked differences in I_a/I_c ratios, from 1 : 1 for **8** down to 0.52 : 1 for **1**, which could be attributable to chemical (so-called EC mechanism) or electrochemical (the rate of heterogenous electron transfer) irreversibility, or a combination of the two. Analysis of the anodic and cathodic current ratios for **1** to **9** was difficult in most cases due to the proximity of the E^2 process. Therefore, we employed the Tomeš criterion to assess electrochemical reversibility (Table S33 in the Supporting Information), measuring the difference at the one-quarter and three-quarter cathodic wave potentials.[67] In an aqueous solution, the

potential difference for a reversible process would be 56.5 mV. Our electrochemistry was done in a low dielectric solvent, and as such it is expected that the potential differences measured will be intrinsically larger, despite the use of 0.4 M supporting electrolyte to mitigate this effect. Hence, the average $\triangle E(^1/_4-^3/_4) = 68$ mV led us to conclude that the first reductions of these aryl SDIs appear to be either Nernstian or close-to-Nernstian in their responses, consistent with sufficiently fast rates of electron transfer relative to the standard CV scan rates employed. Thus, the cases with lower I_a/I_c ratios are attributed to EC processes with follow-on chemical reactions, which consume the produced SDI radical anions at varying rates for different species. This has been correlated to the varying radical anion lifetimes as deduced from the SEEPR experiments (next section).

The above conclusions relating to anion radical stability also bears on the anomalously low currents observed for most E^2 processes, as clearly evident for **1** and **6** in Figure 9. Broadly, two possibilities should be considered. Firstly, for those with shorter lifetimes the time delay to traverse $\Delta E_p^{c(1-2)}$ leads to such a loss of redox-active material that the apparent currents for this second reduction are greatly diminished. Evidence for this was the observation of significant deposits on the working electrodes during cathodic voltammetry experiments. Secondly, if the initial products somehow aggregate to larger species, expected to have smaller diffusion coefficients, this could result in lower fluxes and hence lower peak currents. In this scenario, E^2 (except possibly in the case of **7**) would be measuring a second reduction of *different species*. Support for this potentiality is provided by the reported high reactivity of SDI radical anions.[68] In the original report, scrambling of mixtures of aryl SDIs occurred with a catalytic amount of alkali metal reducing agents. Although originally proposed as *radical couplings* via their π3* SOMOs, a similar process may operate (Figure 11) between one radical and a neutral SDI. While there are no reports that higher aggregated ring- or (branch)chained radicals can be formed by such a process, there are many known examples of rapid changes in molecularity of thiazyl compounds under redox conditions.[1] This could serve as an alternative explanation for the highly unusual appearances of the redox waves we observed for the E^2 processes in **1–6**, **8**, and **9**. A similar concept has been proposed before.[29]

The correlation of E_p^{c1} to the energy of the LUMOs as calculated by DFT, is excellent ($R^2 > 0.97$, Figure 12). This evidence therefore indicates that the reductions of aryl SDIs are strongly redox tunable by suitable variations in substituents. Moreover, the linear fits in Figure 12 will allow reasonable predictions of the reduction potentials of unknown sulfur diimides from relatively straightforward DFT computations. An excellent correlation also exists between E_p^{a3} for oxidation of **1–5**, consistent with the orbital topologies calculated for the HOMOs, but fails for the other exemplars for undetermined reasons.

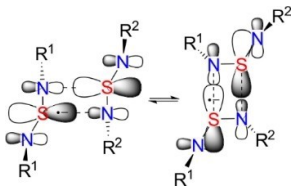

Figure 11. Sulfur diimide radical anion scrambling reaction following Bestari et al.[68b]

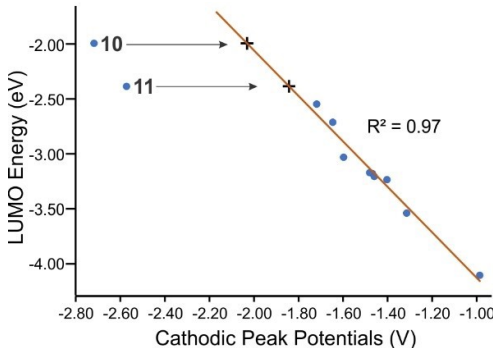

Figure 12. Plot of E_p^{c1} of **1–11** vs DFT LUMO Energies calculated using B3LYP-D3BJ/6-311++G(2d,p), with linear fit through **1–9** and extrapolated points (+) for **10** and **11** to this line.

An interesting question is whether these predictions are also valid for non-aryl SDIs. For the alkyl and silyl compounds **10** and **11** (Table 5 and the Supporting Information), the only process observed is an irreversible reduction ($I_a/I_c = 0$), with strong dependency of E_p^{c1} on scan rate. This is indicative of significantly slowed rates of electron transfer (electrochemical irreversibility) in addition to rapid EC decomposition processes. Importantly, the SEEPR signals were determined under steady-state conditions.[25] A difficulty with irreversible redox processes in voltammetry is that the apparent potentials become functions of the rates of the follow-up reactions in the EC process and become, even more dramatically, dependent on the rates of heterogeneous electron transfer – this is the so-called *overpotential* that readily exceeds many tenths of volts.[69] Clearly, the measured E_p^{c1} of **10** and **11** do not fit to the correlation line for reductions of **1–9** in Figure 12. Do they then belong to a different correlation, of similar slope, at much more negative potentials? Or should we extrapolate E_p^{c1} via their computed LUMO energies (+ marks on the linear fit)? The latter, yielding apparent Nernstian potentials of −2.06 V for **10** and −1.87 V for **11**, at the very least establish a lower limit for these two potentials.

EPR Spectroscopic Results

Electron Paramagnetic Resonance (EPR) spectra were obtained for reduction of the SDIs in this series. The lifetime of SDI radical anions is quite short when electrochemically reduced, requiring the use of simultaneous electrochemical electron paramagnetic resonance (SEEPR). Samples were prepared in quartz flat cells in CH_2Cl_2 with $[^nBu_4N][PF_6]$ supporting electrolyte. Electrodes (working = Pt, reference = Ag, auxiliary = Pt) were placed in the cell and a voltage corresponding to the 0/−1 redox process (as determined by *in situ* SWVs) was applied.[70] For each of **1** to **9**,

this resulted in production of an EPR signal (Figures 13 and S74–S82) which, along with comparable current densities in each CV of **1** to **9**, provides confirmation that all sulfur diimides in this series undergo a one-electron reduction in the first cathodic process.

The lifetimes of the radical species are strongly dependent on the electron-withdrawing abilities of the substituents, with the most electron-donating (methoxy, $\mathbf{1}^{\bullet-}$) having the shortest lifetime, some tens of seconds, and the most electron-withdrawing (nitro, $\mathbf{7}^{\bullet-}$) having a lifetime of minutes. In fact, the strongest signal from $\mathbf{7}^{\bullet-}$ was obtained when electrolysis preceded the EPR scan by ~30 seconds to build up a higher radical concentration. This trend extends to $\mathbf{11}^{\bullet-}$, which under near-identical conditions has a lifetime of <5 seconds due to its highly electron-donating $SiMe_3$ groups, combined with the lack of electron delocalization lent by the aryl rings in **1** to **9**.[25] Hyperfine couplings (HFCs) on the NSN nitrogen atoms decrease from $\mathbf{1}^{\bullet-}$ to $\mathbf{7}^{\bullet-}$ with more electron-withdrawing substituents (Table 6). They increase for the trihaloaryl groups and $\mathbf{9}^{\bullet-}$ has the largest nitrogen HFC in the series, consistent with a higher population of the Z/Z conformation, which tends towards a radical anion more localized on the NSN moiety due to diminished π-delocalization to the aryl rings. The aryl *ortho*-hydrogens of compounds $\mathbf{1}^{\bullet-}$–$\mathbf{7}^{\bullet-}$ have significantly large HFCs, on the order of 3–5.5 MHz (2–4 mT). The *meta*-hydrogens have significantly smaller couplings, except in **2** and **3** where they are 0.8–3.8 MHz (0.6–2.8 mT). This is in full accordance with the expected β coupling due to the $p(\pi)$ spin densities of the attached C atoms (see Figure S84 in the Supporting Information).

Radicals $\mathbf{8}^{\bullet-}$ and $\mathbf{9}^{\bullet-}$ only contain *meta*-hydrogens, and these have small couplings. The EPR spectra of $\mathbf{1}^{\bullet-}$, $\mathbf{4}^{\bullet-}$, $\mathbf{5}^{\bullet-}$, $\mathbf{7}^{\bullet-}$, and $\mathbf{9}^{\bullet-}$ are dominated by the 1:2:3:2:1 pentet, which is consistent with the large spin density localized on the two nitrogen atoms (Figure S84) and the absence of high-abundance isotopes with large gyromagnetic ratios on the aryl groups. Excellent simulated fits for all experimental data were obtained while treating the nitrogen HFC as identical, implying that the conformation of the sulfur diimide radical anions are symmetrical. When running the simulations, the parameters for the nitrogen atoms were initially varied independently, but were found to refine similarly, such that the agreement of the simulation to the experimental data did not worsen when the nitrogen HFC were restricted to identical values. Radicals $\mathbf{2}^{\bullet-}$, $\mathbf{3}^{\bullet-}$, $\mathbf{6}^{\bullet-}$ and $\mathbf{8}^{\bullet-}$ show more complex multiplets that display the influence of strong coupling to aryl-hydrogens and/or aryl- or trifluoromethyl ^{19}F nuclei. The *g*-values do not greatly vary over most of the series (2.0062 to 2.0065) with $\mathbf{5}^{\bullet-}$ and $\mathbf{9}^{\bullet-}$ at 2.0070 and 2.0090 significant outliers, attributable to spin-orbit coupling from the heavy Br nuclei, with an effect that increases in lock step from two to six Br substituents.

For each of the anions $\mathbf{1}^{\bullet-}$–$\mathbf{9}^{\bullet-}$, density functional theory (DFT) calculations were performed on the neutral species at the UB3LYP/6-311++G(2d,p) level of theory with and without the D3BJ post-SCF dispersion correction in the three nominal conformations E/Z, Z/Z and E/E. Some averaged geometrical data is provided in Figure 4C for the first two conformations,

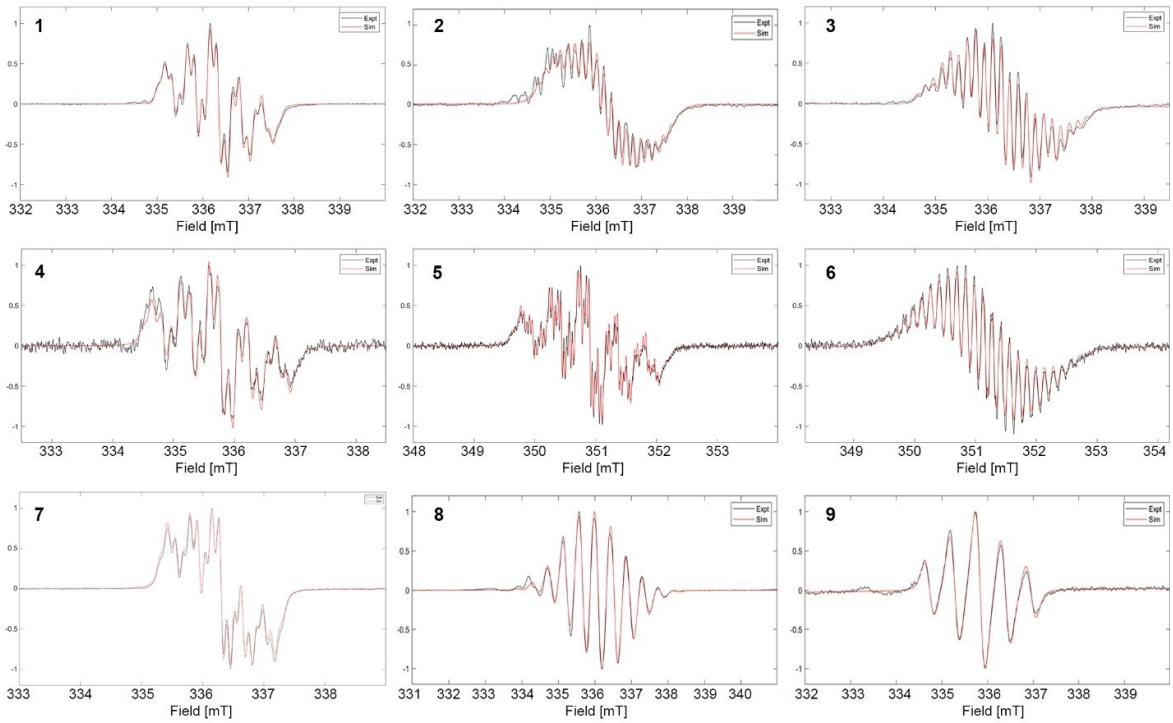

Figure 13. EPR spectral data for $\mathbf{1}^{\bullet-}$ to $\mathbf{9}^{\bullet-}$. Black lines are experimental spectra and red are line-fitted simulations undertaken with EasySpin-5.2.31. The intensities (*y*-axes) are in arbitrary units.

Table 6. Experimental EPR Spectroscopic Data Compared with DFT Computed Values.[a]

Substituents:	OCH_3	CH_3	F	Cl	Br	CF_3	NO_2	F_3	Br_3
g–value	2.0062	2.0063	2.0064	2.0065	2.0070	2.0063	2.0063	2.0065	2.0090
HFC (MHz)									
2 ^{14}N[b]	13.83	13.26	13.70	13.19	13.11	12.28	10.00	12.79	15.65
E/Z	8.16	7.79	8.00	7.53	7.47	7.47	7.47	*11.29*	10.80
Z/Z	19.24	18.94	19.36	18.66	18.69	18.69	18.69	18.40	*17.37*
E/E	7.62	7.24	7.38	7.05	6.99	6.99	6.99	6.87	5.53
E/Z-Z/Z	*13.84*	*13.37*	*13.68*	*13.09*	*13.08*	*12.38*	*9.72*	14.85	14.09
2 ^{1}H[c]	4.32	5.64	4.12	4.19	4.01	4.13	3.73		
E/Z	7.01	6.51	6.87	6.63	6.57	6.57	6.57		
Z/Z	*5.65*	*5.52*	*5.71*	*5.56*	*5.46*	*5.46*	*5.46*		
E/E	5.72	5.95	6.25	5.93	5.88	5.88	5.88		
2 ^{1}H[c]	3.77	4.9	4.12	3.74	3.91	2.9	3.01		
E/Z	4.45	4.33	*4.58*	4.39	*4.35*	4.35	4.35		
Z/Z	4.64	*4.36*	4.64	4.51	4.39	4.39	4.39		
E/E	*3.54*	3.06	3.22	*3.28*	3.26	*3.26*	*3.26*		
2 ^{1}H[d]	1.16	3.73	3.67	1.34	1.6	1.06	0.42	1.42	1.89
E/Z	2.57	*2.73*	2.87	2.83	2.80	2.80	2.80	2.32	*1.43*
Z/Z	2.11	2.11	2.11	2.20	2.15	2.15	2.15	2.67	1.29
E/E	*1.49*	1.67	*1.61*	*1.85*	*1.87*	*1.87*	*1.87*	*2.18*	2.60
2 ^{1}H[d]	1.16	1.59	0.78	1.18	*1.18*	0.89	0.19	1.41	1.63
E/Z	*1.21*	*1.29*	1.36	1.36	1.34	1.34	1.34	1.60	*1.43*
Z/Z	1.96	1.92	2.01	1.98	5.00	1.90	1.90	*1.57*	1.29
E/E	1.46	1.16	*1.32*	*1.15*	5.00	*1.11*	*1.11*	1.88	2.11
*n*X		4.24[e]	9.57[f]			7.92[g]	0.64[h]	11.38[g]	
E/Z		6.89[e]	11.17[f]			15.51[g]	0.98[h]	6.96[g]	
Z/Z		5.78[e]	*9.41*[f]			12.26[g]	*0.91*[h]	4.66[g]	
E/E		*5.33*[e]	8.54[f]			*10.42*[g]	0.97[h]	*8.16*[g]	

[a] An alternate table reports HFS in mT, Table S34, in the Supporting Information. Experimental values are from full line-fitting of the experimental data in EasySpin. Computed HFC values are from UB3LYP-D3BJ/6-311++G(2d,p) calculations based on the conviction that the dispersion correction gives more accurate geometries, even if not always indicating the most stable conformations in solution. HFC have been symmetry averaged to match the experimental signals; full original data are in Table S36 of the Supporting Information. [b] Assigned to the N14 nuclei of NSN bridge. [c] Assigned to *ortho*-H of aryl rings, unable to assign E or Z branch. [d] Assigned to *meta*-H of aryl rings, unable to assign E or Z branch. [e] Assigned to H1 nuclei of the two CH_3 groups. [f]Assigned to *para*-F19 nuclei. [g] Assigned to F19 nuclei of the two CF_3 groups for **6**, and the 2,4,6-F atoms for **8**. [h] Assigned to N14 nuclei of the two NO_2 groups.

and the energetics of the isomeric structures are included in Table 1, while fuller details are provided in the Supporting Information. In the E/Z conformation, the Z-branch SN bond length is computed to increase by 4.2% on reduction to the anion and the E-branch by 4.6% in the monoanion, whilst the corresponding C_{ipso}-N bonds decrease by 2.6 and 2.8%. In the symmetric Z/Z conformer, the SN bonds increase by 4.9% and CN decrease by 2.4%, and ∠(NSN) decrease by a few degrees for each conformer. All these changes are consistent with partial occupancy of the 3π* LUMO of the neutral SDIs (see Figure 6). Interestingly, in the anions **1**$^{\bullet-}$–**7**$^{\bullet-}$, using the full dispersion corrected calculations, the structures minimize to fully planar in E/Z and E/E but the Z/Z conformations maintain essentially the same folded conformation of the neutral species (structures are provided in the Supporting Information, see Tables S47 and S48). Only in the di-*ortho* substituted anions, **8**$^{\bullet-}$ and **9**$^{\bullet-}$, do the Z/Z conformations adopt the close face-to-face aryl ring spacing. Also, in their E/Z isomers, the Z-branch aryl rings are twisted by dihedrals of 39 and 56°, respectively, whereas the E/E isomers adopt the fully co-planar conformation common for aryl SDI anion radicals.

Most interestingly, the computed energies of the conformers in the gas phase (Table 1) provide ambiguous predictions about the 'most stable conformation'. Indeed, the trends from the calculations with and without the D3BJ post-SCF dispersion corrections are effectively mirror images. Ignoring dispersion, the E/Z conformer is almost always the lowest except **8** and **9**, for which E/E is lowest, but the energy differences are negligible, and a mixture of isomers would ensue. Including dispersion, which we consider more accurate despite some expected over-correction, Z/Z and E/Z are within 5 kJ/mol for all except **9**, while E/E is in most cases less favoured

by more significant margins ($\geq$10 kJ/mol). Importantly, the energetic differences are very small, and with the reduced π-bond orders, the anions could reasonably be expected to exist as freely exchanging conformers in solution.

This is further borne out by the EPR spectroscopic results. In all cases, the (dominant) ^{14}N HFC is found to be the same for both nuclei, thus equal nitrogen environments at ambient temperature, whether static or dynamic. The DFT computed HFC constants (Table 6) provide a most interesting outcome: the *general agreement* of all the predicted values with experiment is utterly convincing regarding the identity of these radical anions. But the specific values, radical by radical, vary from nucleus to nucleus over the three limiting conformations used in the computations. Since the ^{14}N HFC are the most prominent in all the spectra and usually the largest in magnitude, we draw attention to the larger than observed prediction of the ^{14}N HFC values for Z/Z and smaller than observed for the other two conformers. Moreover, a simple average of the computed values for this HFC between E/Z and Z/Z (line 6 in Table 6) provide a superb fit to experiment, with deviations (per MHz) of less than 3% for **1–7**. Only for **8** and **9** do the HFC agreements fit closer to a pure Z/Z conformation, consistent with the expected greater dispersion interactions between substituents in these radical anions. Interpretation of these values necessarily must leave a considerable margin: computationally from the inability to accurately predict very flexible radicals; experimentally from the significantly under-parameterized spectral data. Nevertheless, considering the detailed comparison of the HFC computational predictions, the evidence points to radical anions that are present as mixtures of E/Z and Z/Z conformations. Interestingly, a relaxed scan calculation for SN bond rotation, conducted on **3**$^{\bullet-}$, provides a smooth isomerization path with a computed barrier of $<$13 kJ/mol, consistent with a population weighted dynamic average of conformations in solution. Moreover, the timescales of the EPR experiments evidently allow for identification of intact radical anions in solution and do not show the decay of magnetization that might be expected from rapid radical-radical substituent exchange according to the synthetic study of Bestari et al.[68b]

Conclusions

Acyclic sulfur diimides are an important class of delocalized molecules with allylic character that are noteworthy for having a third-period element, sulfur, as the central atom. They have been known for a considerable period but have not been as well studied as closely related organic heterocumulenes. The application of a systematic approach, with full attention to the rich isomeric diversity encountered in solution, the solid state, and amongst different redox states, affords important insights into the redox properties of this class which is of great significance *inter alia* to the behaviour of SDIs as chelating ligands to metals. As shown by systematic voltammetric investigation, supported by SEEPR spectroscopy, this work has characterized the strong redox tunability of aryl SDIs. The linear correlation for the E^1 process provides a reliable index for the redox tuning of any conceivable diaryl SDI. It also provides an absolute lower limit for the thermodynamic redox first reduction potentials of the important SDI ligands **10** and **11**. Whether the alkyl or heteroatom-substituted SDIs are truly more difficult to reduce by as much as one volt remains an open question that can only be resolved by a systematic study by voltammetry of more exemplars of such SDIs.

Experimental Section

Chemical Synthesis. Reagents and general procedures are reported in the Supporting Information, along with a detailed synthetic report for the reliable preparation of all the SDIs discussed in this report. Synthesis of previously unreported **6** and **8** are described here.

Synthesis of bis(4-trifluoromethylphenyl)sulfurdiimide (**6**). 4-trifluoromethylaniline (8.0 mL, 64 mmol) was dissolved in ~50 mL dry benzene and stirred under N_2 flow. To this was added $SOCl_2$ (10 mL, 138 mmol) diluted in 30 mL of benzene. Solid anilinium chloride salt formed on addition of $SOCl_2$ but dissolved with heating. The reaction mixture was refluxed for ~3 hours, until the evolution of HCl vapors ceased. The solvent was removed, leaving a bright yellow oil, which was 4-trifluoromethyl-N-sulfinylaniline. Yield: 11.4 g, 86%. ^{1}H NMR (300 MHz, $CDCl_3$): δ = 7.68 ppm (d; ^{3}J(H,H) = 8.7 Hz, 2ArH), 7.91 ppm (d; ^{3}J(H,H) = 8.4 Hz, 2ArH). ^{19}F{^{1}H} NMR (282 MHz, $CDCl_3$): δ = −62 ppm (s, CF_3).

Dissolved 4-trifluoromethyl-N-sulfinylaniline (9.07 g, 43.8 mmol) in dry toluene, and stirred under N_2 flow. On addition of potassium *tert*-butoxide (3.68 g, 33 mmol), the solution immediately turned dark red. The mixture was refluxed for 4 hours, after which the toluene was removed. The remainder was dissolved in pentane, and then filtered under N_2. The pentane was then removed, leaving a dark red oil. This was distilled under vacuum (115 °C). The distillate contains the impurities of the crude product, leaving sulfur diimide behind in the boiling flask. Yield: 4.29 g, 56%. ^{1}H NMR (700 MHz, $CDCl_3$): δ = 7.42 ppm (d; ^{3}J(H,H) = 8.1 Hz, 4H, *o*-ArH), 7.57 ppm (d; ^{3}J(H,H) = 8.4 Hz, 4H, *m*-ArH). ^{13}C{^{1}H} NMR (176 MHz, $CDCl_3$): δ = 123.2 ppm (s, 4 C, *o*-ArC), 124.1 ppm (q, ^{1}J(C,F) = 272 Hz, 2 C, CF_3), 126.4 ppm (q, ^{3}J(C,F) = 3.7 Hz, 4 C, *m*-ArC), 128.9 ppm (q, ^{2}J(C,F) = 32.8 Hz, 2 C, *p*-ArC), 147.7 ppm (q, ^{5}J(C,F) = 1.4 Hz, 2 C, *i*-ArC). ^{19}F NMR (282 MHz, $CDCl_3$): δ = −62 ppm (s, 6F, CF_3). FTIR (cm^{-1}): 3221, 2934, 1911, 1670, 1608, 1575, 1504, 1413, 1388, 1318, 1273, 1236, 1161, 1103, 1066, 1049, 1012, 967, 904, 874, 841, 755, 736, 717, 654, 636, 595, 570, 513, 436. MP: 37.2–39.5 °C. Anal. Calcd for $C_{14}H_8F_6N_2S$: C, 48.00; H, 2.30; N, 8.00; S, 9.15%. Found: C, 48.18; H, 2.09; N, 8.36; S, 8.90%.

Synthesis of bis(2,4,6-trifluorophenyl)sulfurdiimide (**8**). In a round-bottomed side-arm flask, 2,4,6-trifluoroaniline (2.04 g, 13.9 mmol) was dissolved in ~80 mL dry benzene and stirred under N_2 flow. To this was added $SOCl_2$ (2.2 mL, 30 mmol) diluted in ~20 mL of benzene. The reaction mixture was refluxed for ~2.5 hours, until the evolution of HCl vapors ceased. Removed solvent to yield a dark yellow oil, 2,4,6-trifluorophenyl-N-sulfinylaniline. Yield: 2.12 g, 79%. ^{1}H NMR (300 MHz, $CDCl_3$): δ = 6.83 ppm (m; 2ArH); ^{19}F NMR (282 MHz, $CDCl_3$): δ = −105 ppm (m; 1F; *p*-ArF), −107 ppm (m; 2F; *o*-ArF).

In a round-bottomed side-arm flask, 2,4,6-trifluorophenyl-N-sulfinylaniline (2.12 g, 11.0 mmol) was dissolved in ~100 mL dry benzene, and potassium *tert*-butoxide (0.7 g, 6.2 mmol) was added. This was stirred at RT, changing colour from pale yellow to a medium orange solution. Upon reflux, the solution turned dark yellow. Refluxed for 2.5 hours, then cooled to RT, leaving a dark gel-like substance. This

was washed three times with dH_2O, the organic phase was separated, dried over $MgSO_4$, and solvent was removed. The resulting brown crystals were >99% pure sulfur diimide, as indicated by ^{1}H NMR. Yield: 1.49 g, 84%. ^{1}H NMR (700 MHz, $CDCl_3$): δ = 6.52 ppm (4H; t; *m*-ArH). $^{13}C\{^1H\}$ NMR (176 MHz, $CDCl_3$): δ = 99.9 ppm (ddd, $^2J(C,F) = 26.6$ Hz, $^2J(C,F) = 23.6$ Hz, $^4J(C,F) = 4.8$ Hz, 4 C, *m*-ArC), 117.9 ppm (td, $^2J(C,>F) = 17.7$ Hz, $^4J(C,F) = 5.1$ Hz, 2 C, *i*-ArC), 153.6 ppm (ddd, $^1J(C,F) = 252.3$ Hz, $^3J(C,F) = 14.7$ Hz, $^3J(C,F) = 7.0$ Hz, 4 C, *o*-ArC), 160.3 ppm (dt, $^1J(C,F) = 250.6$ Hz, $^3J(C,F) = 14.4$ Hz, 2 C, *p*-ArC). ^{19}F NMR (282 MHz, $CDCl_3$): δ = −109 ppm (m; 2F; *p*-ArF), −113 ppm (m; 4F; *o*-ArF). FTIR (cm^{-1}): 510, 835, 985, 1038, 1123, 1267, 1443, 1486, 1605, 3105. MP: 95.9–96.5 °C. Anal. Calcd for $C_{12}H_4F_6N_2S$: C, 44.73; H, 1.25; N, 8.69; S, 9.95%. Found: C, 44.72; H, 1.11; N, 8.99; S, 11.61%.

Crystallography. Crystals were selected under a polarizing microscope and checked for optical extinction. Colourless or pale-yellow crystals were mounted in Fomblin™ oil on 100 μm MiTeGen loops and cooled to 173(2) or 100(1) K using the diffractometer cooling devices. Data were collected either on Bruker ApexII CCD (Mo Kα) or Rigaku-Oxford Diffraction SuperNova HPC (Cu Kα) diffractometers. Data collection and reduction was controlled, respectively, with *SAINT-Plus* or CrysAlisPro 1.171.38.43 (Rigaku Oxford Diffraction, 2021). The data were processed and corrected for Lorentz and polarization effects by standard methods and corrected for absorption by semi-empirical methods from equivalents. Structures were solved with ShelXT[71] and refined using Levenberg–Marquardt minimization with olex2.refine within the Olex2 suite of programs.[42] The refinements employed NoSpherA2, (NOn-SPHERical Atom-form-factors in Olex2)[41] an implementation of HAR that makes use of tailor-made aspherical atomic form factors calculated on-the-fly from a Hirshfeld-partitioned electron density (ED). The ED is calculated from a Gaussian basis set single determinant SCF wavefunction in DFT at the PBE/def2-TZVP level of theory using ORCA 4.5. Crystal data and structure refinement parameters are summarized in Table S1 in the SI, and full archival data is available in CIF format.

Voltammetry. Cyclic (CV) and square-wave (SWV) voltammetry experiments were performed with a Princeton Applied Research PARSTAT 2273 potentiostat using the PowerSuite software version 2.58, and the embedded PowerCV software version 2.46. Experiments were done in a nitrogen-filled MBraun glovebox with oxygen and moisture rigorously excluded. The working electrode used was a glassy-carbon inlaid-disk electrode with a surface area of 7.1 mm^2, the reference electrode was silver wire, and the counter electrode was a coiled platinum wire. Dichloromethane was initially dried by distillation from CaH_2 under nitrogen and subsequently freeze-thaw degassed before transfer to the glovebox.

Simultaneous Electrochemical EPR (SEEPR). SEEPR experiments were conducted in $CH_2Cl_2/[^nBu_4N][PF_6]$ by using a miniature Wilmad WG-808 quartz electrolytic flat cell with platinum foil working electrode, Teflon-coated silver reference electrodes, and a platinum wire auxiliary electrode. The Bruker EMX Plus EPR spectrometer was operating at X-band frequencies (9.8 GHz) and during electrolysis the spectra were monitored in intensity-versus-field mode. The spectra were simulated using EasySpin 5.2.31 software within the MatLab software suite.

Computation. Computations were carried out by Gaussian 16 W V1.1 using the GaussView 6.0.16 GUI. The functional used was B3LYP, with a 6-311++G(2d,p) basis set. D3BJ dispersion correction was used when indicated. PCM CH_2Cl_2 solvent model was used when indicated. For UV-vis simulations (e.g. Figure 8), a single-point calculation CAMB3LYP-D3BJ/6-311++G(2d,p) was applied to the geometry-optimized structures calculated by B3LYP-D3BJ/6-311++G(2d,p) method. Vibrational spectra (IR and Raman) were computed using the frequency calculation in Gaussian 16 W, including ^{15}N isotope substitution. Gaussian relaxed scan techniques as well as IRC calculations were undertaken, using the standard method including dispersion correction, to assess the mechanisms of isomer interconversion.

Supporting Information

(See footnote on the first page of this article): Full synthetic experimental details; Full crystallographic details; Assessment of the HAR/NoSpherA2 refinement approach; Comparison of SC-XRD to DFT computed geometries; NMR spectroscopy data tables; computed isomerization pathways; voltammetry data tables and figures; frontier MOs; EPR data and figures; UV-vis tables and figures; TD-DFT derived simulations for UV-Vis; FTIR data tables and figures; archival NMR spectra; DFT optimized geometry Cartesian coordinates. Movie files visualizing several IRC calculations. Deposition Numbers 1578020 (**1**), 1578021 (**2**), 1578022 (**3**), 1578023 (**4**), 1578024 (**5**), 2022775 (**6**), 1578025 (**7**), 1889021 (**8**), 1889023 (**9**), 1578027 (**15**) and 1961561 (**16**) contain the supplementary crystallographic data for this paper. These data are provided free of charge by the joint Cambridge Crystallographic Data Centre and Fachinformationszentrum Karlsruhe Access Structures service. The authors have cited additional references within the Supporting Information (Ref. [72]).

Acknowledgements

The authors gratefully acknowledge financial support from the Natural Sciences and Engineering Research Council (Canada) and to the University of Lethbridge and the Faculty of Arts and Science for purchasing the X-ray diffractometer. The Canadian Foundation for Innovation and the Government of Alberta funded the EPR Spectrometer. N.D.D.H. thanks the University of Lethbridge, the Government of Alberta, the University of Lethbridge Graduate Student Association and the Dr Barbara June Whitlock Chemistry Scholarship for graduate stipends. We thank the anonymous reviewers for some very helpful suggestions, which have significantly improved the article.

Conflict of Interests

The authors declare no conflicts of interest.

Data Availability Statement

The data that support the findings of this study are available in the supplementary material of this article.

Keywords: thiazyl chemistry · electrochemistry · chemical synthesis · EPR spectroelectrochemistry · DFT computation · SC-

XRD structure determination · infrared spectroscopy · UV-vis spectroscopy

[1] T. Chivers, R. S. Laitinen, *Chalcogen-nitrogen Chemistry: From Fundamentals To Applications In Biological, Physical And Materials Sciences (Updated Edition)*, World Scientific Publishing Company, **2021**, Ch. 1o, pp. 229–269.
[2] M. Goehring, G. Weis, *Angew. Chem.* **1956**, *68*, 678.
[3] a) U. Wannagat, H. Kuckertz, *Angew. Chem.* **1962**, *74*, 117–118; b) M. Herberhold, G. Silke, B. Wrackmeyer, *Phosphorus Sulfur Silicon Relat. Elem.* **1992**, *66*, 273–283.
[4] a) D. H. Clemens, A. J. Bell, J. L. O'Brien, *Tetrahedron Lett.* **1965**, *20*, 1487–1489; b) D. H. Clemens, A. J. Bell, J. L. O'Brien, *Tetrahedron Lett.* **1965**, *6*, 1491–1495; c) R. Appel, J. Kohnek, *Chem. Ber.* **1970**, *103*, 2152–2156; d) A. Senning, *Sulfur Lett.* **1991**, *13*, 97–100.
[5] R. Cramer, *J. Org. Chem.* **1961**, *26*, 3476–3478.
[6] a) R. Fleischer, D. Stalke, *Coord. Chem. Rev.* **1998**, *176*, 431–450; b) J. Valjus, H. M. Tuononen, R. S. Laitinen, *Can. J. Chem.* **2018**, *96*, 591–598; c) D. Lüert, C. M. Legendre, R. Herbst-Irmer, D. Stalke, *Chem. Eur. J.* **2022**, *28*, e202104470.
[7] a) J. L. Morris, C. W. Rees, D. J. Rigg, *J. Chem. Soc. Chem. Commun.* **1985**, *7*, 396–397; b) C. Habben, A. Meller, *Chem. Ber.* **1986**, *119*, 9; c) C. Hubrich, A. Schulz, A. Villinger, *Z. Anorg. Allg. Chem.* **2007**, *633*, 2362–2366.
[8] a) G. Kresze, W. Wucherpfennig, *Angew. Chem. Int. Ed.* **1967**, *6*, 149–167; b) A. V. Zibarev, G. G. Yakobson, *Russ. Chem. Rev.* **1985**, *54*, 1006–1024.
[9] M. Andresini, M. Colella, L. Degennaro, R. Luisi, *Org. Biomol. Chem.* **2023**, *21*, 7681–7690.
[10] J. P. Donahue, *Chem. Rev.* **2006**, *106*, 4747–4783.
[11] a) J. Henn, D. Ilge, D. Leusser, D. Stalke, B. Engels, *J. Phys. Chem. A* **2004**, *108*, 9442–9452; b) D. Leusser, J. Henn, N. Kocher, B. Engels, D. Stalke, *J. Am. Chem. Soc.* **2004**, *126*, 1781–1793; c) R. Gleiter, G. Haberhauer, *Coord. Chem. Rev.* **2017**, *344*, 263–298.
[12] V. H. H. Hoerhold, J. Beck, *J. Prakt. Chem.* **1969**, *311*, 621–629.
[13] a) A. V. Zibarev, *Heteroat. Chem.* **1990**, *1*, 443; b) I. Y. Bagryanskaya, Y. V. Gatilov, M. M. Shakirov, A. V. Zibarev, *Mendeleev Commun.* **1994**, *4*, 136–137; c) I. Y. Bagryanskaya, Y. V. Gatilov, A. V. Zibarev, *J. Struct. Chem.* **1997**, *38*, 829–845; d) I. Y. Bagryanskaya, Y. V. Gatilov, A. V. Zibarev, *J. Struct. Chem.* **1999**, *40*, 640–643.
[14] N. E. Petrachenko, V. I. Vovna, A. V. Zibarev, G. G. Furin, *Russ. J. Gen. Chem.* **1993**, *63*, 921–925.
[15] a) M. Wang, F. Wudl, *J. Mater. Chem.* **2010**, *20*, 5659–5663; b) M. Wang, Y. Sun, M. Tong, E. S. Chesnut, J. H. Seo, R. Kumar, F. Wudl, *J. Polym. Sci. Part A* **2010**, *49*, 441–451.
[16] R. L. Melen, D. J. Eisler, R. A. Hewitt, J. M. Rawson, *Dalton Trans.* **2013**, *42*, 3888–3895.
[17] a) B. A. D. Neto, P. H. P. R. Carvalho, J. R. Correa, *Acc. Chem. Res.* **2015**, *48*, 1560–1569; b) J. Zhang, T. C. Parker, W. Chen, L. Williams, V. N. Khrustalev, E. V. Jucov, S. Barlow, T. V. Timofeeva, S. R. Marder, *J. Org. Chem.* **2016**, *81*, 360–370; c) M. A. Kolaczkowski, A. Garzon-Ruiz, A. Patel, Z. Zhao, Y. Guo, A. Navarro, Y. Liu, *ACS Appl. Mater. Interfaces* **2020**, *12*, 53328–53341.
[18] D. G. Patel, F. Feng, Y. Y. Ohnishi, K. A. Abboud, S. Hirata, K. S. Schanze, J. R. Reynolds, *J. Am. Chem. Soc.* **2012**, *134*, 2599–2612.
[19] S. Grabowsky, P. Luger, J. Buschmann, T. Schneider, T. Schirmeister, A. N. Sobolev, D. Jayatilaka, *Angew. Chem. Int. Ed. Engl.* **2012**, *51*, 6776–6779.
[20] a) J. A. Hunter, B. King, W. E. Lindsell, M. A. Neish, *J. Chem. Soc. Dalton Trans.* **1980**, 880–887; b) A. Klein, C. Vogler, W. Kaim, *Organometallics* **1996**, *15*, 236–244.
[21] G. Li, H. Yang, F. Li, F. Cheng, W. Shi, J. Chen, P. Cheng, *Inorg. Chem.* **2016**, *55*, 4935–4940.
[22] N. M. Bonanno, N. Van Damme, A. J. Lough, M. T. Lemaire, *Dyes Pigm.* **2015**, *123*, 212–217.
[23] T. Kambe, R. Sakamoto, K. Hoshiko, K. Takada, M. Miyachi, J. H. Ryu, S. Sasaki, J. Kim, K. Nakazato, M. Takata, H. Nishihara, *J. Am. Chem. Soc.* **2013**, *135*, 2462–2465.
[24] B. L. Small, M. Brookhart, *J. Am. Chem. Soc.* **1998**, *120*, 7143–7144.
[25] S. V. Klementyeva, N. P. Gritsan, M. M. Khusniyarov, A. Witt, A. A. Dmitriev, E. A. Suturina, N. D. D. Hill, T. L. Roemmele, M. T. Gamer, R. T. Boeré, P. W. Roesky, A. V. Zibarev, S. N. Konchenko, *Chem. Eur. J.* **2017**, *23*, 1278–1290.
[26] F. T. Edelmann, *Coord. Chem. Rev.* **2018**, *370*, 129–223.
[27] K. Kaleta, M. Ruhmann, O. Theilmann, S. Roy, T. Beweries, P. Arndt, A. Villinger, E. D. Jemmis, A. Schulz, U. Rosenthal, *Eur. J. Inorg. Chem.* **2012**, *2012*, 611–617.
[28] T. Gehrmann, M. Kruck, H. Wadepohl, L. H. Gade, *Chem. Commun.* **2012**, *48*, 2397–2399.
[29] G. Brands, A. Golloch, *Z. Naturforsch., B: J. Chem. Sci.* **1982**, *37*, 1137–1143.
[30] a) R. T. Boeré, K. H. Moock, S. Derrick, W. Hoogerdijk, K. Preuss, J. Yip, M. Parvez, *Can. J. Chem.* **1993**, *71*, 473–486; b) R. T. Boeré, K. H. Moock, M. Parvez, *Z. Anorg. Allg. Chem.* **1994**, *620*, 1589–1598; c) R. T. Boeré, K. H. Moock, *J. Am. Chem. Soc.* **1995**, *117*, 4755–4760; d) R. T. Boeré, T. L. Roemmele, *Coord. Chem. Rev.* **2000**, *210*, 369–445; e) R. T. Boeré, T. L. Roemmele, X. Yu, *Inorg. Chem.* **2011**, *50*, 5123–5136; f) X. Yu, T. L. Roemmele, R. T. Boeré, *ChemElectroChem* **2018**, *5*, 968–978.
[31] U. Wannagat, H. Kuckertz, *Angew. Chem. Int. Ed.* **1962**, *1*, 113.
[32] L. S. Konstantinova, K. A. Lysov, O. A. Rakitin, *Synthesis* **2013**, *45*, 655–658.
[33] E. Lork, R. Mews, M. M. Shakirov, P. G. Watson, A. V. Zibarev, *Eur. J. Inorg. Chem.* **2001**, 2123–2134.
[34] V. Busetti, *Acta Crystallogr., Sect. B: Struct. Crystallogr. Cryst. Chem.* **1982**, *38*, 665–667.
[35] I. Y. Bagryanskaya, Y. V. Gatilov, A. V. Zibarev, *Mendeleev Commun.* **1999**, *9*, 157–158.
[36] a) V. Busetti, G. Cevasco, G. Leandri, *Z. Kristallogr.* **1991**, *197*, 41–50; b) I. Y. Bagryanskaya, Y. V. Gatilov, M. M. Shakirov, A. V. Zibarev, *Mendeleev Commun.* **1994**, *4*, 167–169; c) I. Y. Bagryanskaya, Y. V. Gatilov, E. Lork, R. Mews, M. M. Shakirov, Paul G. Watson, A. V. Zibarev, *J. Fluorine Chem.* **2002**, *116*, 149–156.
[37] S. L. Hinchley, P. Trickey, H. E. Robertson, B. A. Smart, D. W. H. Rankin, D. Leusser, B. Walfort, D. Stalke, M. Bühl, S. J. Obrey, *J. Chem. Soc., Dalton Trans.* **2002**, 4607–4616.
[38] M. Herberhold, S. Gerstmann, B. Wrackmeyer, H. Borrmann, *J. Chem. Soc. , Dalton Trans* **1994**, 633–636.
[39] G. Leandri, V. Busetti, G. Valle, M. Mammi, *J. Chem. Soc. D* **1970**, 413–414.
[40] C. R. Groom, I. J. Bruno, M. P. Lightfoot, S. C. Ward, *Acta Crystallogr., Sect. B: Struct. Sci., Cryst. Eng. Mater.* **2016**, *72*, 171–179.
[41] F. Kleemiss, O. V. Dolomanov, M. Bodensteiner, N. Peyerimhoff, L. Midgley, L. J. Bourhis, A. Genoni, L. A. Malaspina, D. Jayatilaka, J. L. Spencer, F. White, B. Grundkotter-Stock, S. Steinhauer, D. Lentz, H. Puschmann, S. Grabowsky, *Chem. Sci.* **2020**, *12*, 1675–1692.
[42] O. V. Dolomanov, L. J. Bourhis, R. J. Gildea, J. A. K. Howard, H. Puschmann, *J. Appl. Crystallogr.* **2009**, *42*, 339–341.
[43] a) N. D. D. Hill, E. Lilienthal, C. O. Bender, R. T. Boeré, *J. Org. Chem.* **2022**, *87*, 16213–16229; b) M. A. Ibrahim, R. T. Boeré, *New J. Chem.* **2022**, *46*, 5479–5488; c) F. Marszaukowski, R. T. Boeré, K. Wohnrath, *Cryst. Growth Des.* **2022**, *22*, 2512–2533.
[44] R. T. Boeré, *ACS Omega* **2018**, *3*, 18170–18180.
[45] T. L. Roemmele, F. R. Knight, E. Crawford, S. D. Robertson, B. E. Bode, M. Bühl, A. M. Z. Slawin, J. D. Woollins, R. T. Boeré, *New J. Chem.* **2022**, *46*, 22363–22383.
[46] a) J. Kuyper, K. Vrieze, *J. Organomet. Chem.* **1975**, *86*, 127–138; b) R. D. Suenram, F. J. Lovas, W. J. Stevens, *J. Mol. Spectrosc.* **1985**, *112*, 482–493; c) W. Sicinska, L. Stefaniak, M. Witanowski, G. A. Webb, *J. Mol. Struct.* **1987**, *158*, 57–68; d) B. Wrackmeyer, C. Köhler, M. Herberhold, *Magn. Reson. Chem.* **1993**, *31*, 987–990; e) M. Herberhold, S. Gerstmann, W. Milius, B. Wrackmeyer, H. Borrmann, *Phosphorus Sulfur Silicon Relat. Elem.* **1996**, *112*, 261–279.
[47] B. Wrackmeyer, C. Koehler, M. Herberhold, *Magn. Reson. Chem.* **1993**, *31*, 987–990.
[48] R. M. Silverstein, F. X. Webster, D. J. Kiemle *Spectrometric Identification of Organic Compounds*, 7th ed., John Wiley and Sons, New York, **2005**, p. 223.
[49] G. Kresze, M. Berger, P. K. Claus, W. Rieder, *Org. Magn. Reson.* **1976**, *8*, 170–172.
[50] M. Zahedi, S. Shahbazian, S. Weng Ng, *J. Mol. Struct.: THEOCHEM* **2003**, *629*, 91–104.
[51] J. D. Masuda, L. Mokhtabad Amrei, R. T. Boeré, *Eur. J. Inorg. Chem.* **2023**, *26 (33)*, e202300495.
[52] D. Stalke, *Chem. Commun. (Camb.)* **2012**, *48*, 9559–9573.
[53] a) L. Pauling, *J. Am. Chem. Soc.* **1931**, *53*, 1367–1400; b) D. E. Woon, T. H. Dunning, *J. Phys. Chem. A* **2009**, *113*, 7915–7926.
[54] L. Pauling, *The Nature of the Chemical Bond and the Structure of Molecules and Crystals: An Introduction to Modern Structural Chemistry*, Cornell University Press, **1960**, 193–194.

[55] R. T. Boeré, T. L. Roemmele, *Chalcogen–Nitrogen Radicals. In: J. Reedijk, K. R. Poeppelmeier, Comprehensive Inorganic Chemistry II: From Elements to Applications*, Vol. 1. Oxford: Elsevier Science; **2013**. p. 375–411.
[56] a) T. Strassner, J. Fabian, *J. Phys. Org. Chem.* **1997**, *10*, 33–41; b) J. Fabian, *J. Mol. Struct.* **1997**, *10*, 411–416; c) N. Sandblom, T. Ziegler, T. Chivers, *Inorg. Chem.* **1998**, *37*, 354–359; d) A. Modelli, M. Venuti, F. Scagnolari, D. Jones, *Chem. Phys. Lett.* **2001**, *346*, 492–496; e) A. Modelli, M. Venuti, F. Scagnolari, M. Contento, *J. Phys. Chem. A* **2001**, *105*, 219–226; f) J. Hee Lee, I. Lee, C. Kyung Kim, B.-S. Lee, H. Whang Lee, *New J. Chem.* **2002**, *26*, 1693–1697; g) H. M. Tuononen, R. J. Suontamo, J. U. Valkonen, R. S. Laitinen, T. Chivers, *Inorg. Chem.* **2003**, *42*, 2447–2454; h) M. Zahedi, S. Shahbazian, S. W. Ng, *J. Mol. Struct.* **2003**, *636*, 229–240; i) S. Shahbazian, M. Zahedi, S. Weng Ng, *J. Mol. Struct.* **2004**, *673*, 211–221; j) S. Shahbazian, M. Zahedi, *J. Mol. Struct.* **2004**, *683*, 195–206; k) S. Shahbazian, M. Zahedi, S. W. Ng, *J. Mol. Spectrosc.* **2004**, *223*, 195–204; l) S. Shahbazian, R. Firouzi, M. Zahedi, *Theor. Chem. Acc.* **2006**, *117*, 153–161; m) J. Oláh, F. Blockhuys, T. Veszprémi, C. Van Alsenoy, *Eur. J. Inorg. Chem.* **2006**, 69–77; n) E. V. Bartashevich, M. R. Abdrakhmanova, V. A. Potemkin, I. Y. Bagryanskaya, *J. Struct. Chem.* **2006**, *47*, 114–119.
[57] L. Carlsen, H. Egsgaard, *Sulfur Lett.* **1985**, *3*, 87–93.
[58] M. Bayram, D. Bläser, C. Wölper, S. Schulz, *Organometallics* **2015**, *34*, 3421–3427.
[59] a) B. Cohen, A. G. MacDiarmid, *J. Chem. Soc. A* **1966**, 1780–1784; b) H. H. Hörhold, K.-D. Floßmann, *Z. Chem.* **1967**, *7*, 345–346; c) R. Meij, A. Oskam, D. J. Stufkens, *J. Mol. Struct.* **1979**, *51*, 37–49; d) Y.-X. Ding, W. P. Weber, *J. Org. Chem.* **1987**, *52*, 4625–4626; e) C. P. Warrens, J. D. Woollins, M. Witt, H. W. Roesky in *Silicon and Tin Sulfur-Nitrogen Compounds, $(Me_3Si)_2N_2S$, $(Me_3Sn)_2N_2S$, and $(Me_2Sn)S_2N_2$*, **1989**, pp. 43–47.
[60] A. Haas, U. Fleischer, M. Mätschke, V. Staemmler, *Z. Anorg. Allg. Chem.* **1999**, *625*, 681–692.
[61] K. Raghavachari, R. C. Haddon, *J. Phys. Chem.* **1983**, *87*, 1308–1312.
[62] S. Maeda, Y. Harabuchi, Y. Ono, T. Taketsugu, K. Morokuma, *Int. J. Quantum Chem.* **2015**, *115*, 258–269.
[63] a) J. Hine, *J. Am. Chem. Soc.* **1966**, *88*, 5525–5528; b) J. Hine, *J. Org. Chem.* **1966**, *31*, 1236–1244; c) J. Hine in *The Principle of Least Nuclear Motion, Vol. 15* Eds.: V. Gold, D. Bethel), Academic Press, **1977**, pp. 1–61.
[64] J. Fabian, R. Mayer, S. Bleisch, *Phosphorus Sulfur Relat. Elem.* **1979**, *7*, 61–67.
[65] G. Gritzner, J. Kuta, *Pure Appl. Chem.* **1984**, *56*, 461–466.
[66] a) A. J. D. Magenau, Y. Kwak, K. Schroeder, K. Matyjaszewski, *ACS Macro Lett.* **2012**, *1*, 508–512; b) P. R. Murray, S. Crawford, A. Dawson, A. Delf, C. Findlay, L. Jack, E. J. McInnes, S. Al-Musharafi, G. S. Nichol, I. Oswald, L. J. Yellowlees, *Dalton Trans.* **2012**, *41*, 201–207.
[67] a) K. Oldham, J. Myland, A. Bond, *Electrochemical Science and Technology: Fundamentals and Applications*, Wiley, **2011**, p. 252–254; b) A. J. Bard, L. R. Faulkner, H. S. White, *Electrochemical Methods: Fundamentals and Applications*, Wiley, **2022**.
[68] a) R. T. Oakley, *Progress in Inorganic Chemistry, Volume 36*, Wiley, **1988**, p. 299–374; b) K. Bestari, R. T. Oakley, *Can. J. Chem.* **1991**, *69*, 94–99.
[69] a) E. M. Espinoza, J. A. Clark, J. Soliman, J. B. Derr, M. Morales, V. I. Vullev, *J. Electrochem. Soc.* **2019**, *166*, H3175; b) C. Sandford, M. Edwards, K. Klunder, D. Hickey, M. Li, K. Barman, M. Sigman, H. White, S. Minteer, *Chem. Sci.* **2019**, *10*, 6404–6422; c) H. Wang, S. Y. Sayed, E. J. Luber, B. C. Olsen, S. M. Shirurkar, S. Venkatakrishnan, U. M. Tefashe, A. K. Farquhar, E. S. Smotkin, R. L. McCreery, J. M. Buriak, *ACS Nano* **2020**, *14*, 2575–2584.
[70] R. T. Boeré, A. M. Bond, T. Chivers, S. W. Feldberg, T. L. Roemmele, *Inorg. Chem.* **2007**, *46*, 5596–5607.
[71] G. Sheldrick, *Acta Crystallogr. Sect. A* **2015**, *71*, 3–8.
[72] a) E. O. Schlemper, J. Konnert, *Acta Crystallogr.* **1967**, *22*, 918; b) A. T. Christensen, K. O. Stromme, *Acta. Crystallogr., Sect. B: Struct. Crystallogr. Cryst. Chem.* **1969**, *25*, 657–664; c) J. R. Grunwell, W. C. Danison Jr, *Tetrahedron* **1971**, *27*, 5315–5321; d) J. R. Grunwell, C. F. Hoyng, J. A. Rieck, *Tetrahedron Lett.* **1973**, *26*, 2421–2423; e) J. Kuyper, K. Vrieze, *J. Organomet. Chem.* **1974**, *74*, 289–305; f) G. B. Deacon, C. M. Forsyth, N. M. Scott, *Eur. J. Inorg. Chem.* **2000**, *2000*, 2501–2506; g) G. B. Deacon, C. M. Forsyth, N. M. Scott, *J. Chem. Soc., Dalton Trans.* **2001**, 2494–2501; h) A. L. Spek, *J. Appl. Crystallogr.* **2002**, *36*, 7–13; i) C. Elschenbroich, M. Pietras, K. Harms, *J. Organomet. Chem.* **2003**, *684*, 359–367; j) A. L. Spek, *Acta Crystallogr. Sect. D* **2009**, *65*, 148–155; k) F. H. Allen, I. J. Bruno, *Acta Crystallogr. Sect. B* **2010**, *66*, 380–386; l) X. Lin, Z. Zhang, L. Chen, F. Zeng, Y. Luo, C. Xu, *J. Organomet. Chem.* **2014**, *749*, 251–254; m) G. M. Sheldrick, *Acta Crystallogr. Sect. C* **2015**, *71*, 3–8; n) M. Bolte, *CSD Communication (Private Communication)* **2020**; o) F. Neese, *Wiley Interdiscip. Rev.: Comput. Mol. Sci.* **2022**, *12*, e1606; p) R. T. Boeré, *Crystals* **2023**, *13*, 293; q) S. S. Kondage, T. L. Roemmele, R. T. Boeré, *Synlett* **2023**, *34*, 1113–1121; r) V. G. B. do Rosario, F. Marszaukowski, I. Dimbarre Lao Guimarães, F. Gobbo Maranha, B. Francieli Mika, G. Bonifácio Rosa, C. Andrade Pessôa, R. Augusto Pontes Ribeiro, J. Inaba, R. T. Boeré, K. Wohnrath, *Inorg. Chim. Acta* **2023**, *558*, 121749.

Manuscript received: February 9, 2024
Accepted manuscript online: March 5, 2024
Version of record online: March 22, 2024